Circulation Research

ORIGINAL RESEARCH

TXNIP Suppresses the Osteochondrogenic Switch of Vascular Smooth Muscle Cells in Atherosclerosis

Sang-Ho Woo,* Dongsoo Kyung,* Seung Hyun Lee, Kyu Seong Park, Minkyu Kim, Kibyeong Kim, Hyo-Jung Kwon, Young-Suk Won, Inpyo Choi, Young-Jun Park, Du-Min Go, Jeong-Seop Oh, Won Kee Yoon, Seung Sam Paik, Ji Hyeon Kim, Yong-Hwan Kim, Jae-Hoon Choi, Dae-Yong Kim

BACKGROUND: The osteochondrogenic switch of vascular smooth muscle cells (VSMCs) is a pivotal cellular process in atherosclerotic calcification. However, the exact molecular mechanism of the osteochondrogenic transition of VSMCs remains to be elucidated. Here, we explore the regulatory role of TXNIP (thioredoxin-interacting protein) in the phenotypical transitioning of VSMCs toward osteochondrogenic cells responsible for atherosclerotic calcification.

METHODS: The atherosclerotic phenotypes of *Txnip*$^{-/-}$ mice were analyzed in combination with single-cell RNA-sequencing. The atherosclerotic phenotypes of *Tagln*-Cre; *Txnip*$^{flox/flox}$ mice (smooth muscle cell-specific *Txnip* ablation model), and the mice transplanted with the bone marrow of *Txnip*$^{-/-}$ mice were analyzed. Public single-cell RNA-sequencing dataset (GSE159677) was reanalyzed to define the gene expression of TXNIP in human calcified atherosclerotic plaques. The effect of TXNIP suppression on the osteochondrogenic phenotypic changes in primary aortic VSMCs was analyzed.

RESULTS: Atherosclerotic lesions of *Txnip*$^{-/-}$ mice presented significantly increased calcification and deposition of collagen content. Subsequent single-cell RNA-sequencing analysis identified the modulated VSMC and osteochondrogenic clusters, which were VSMC-derived populations. The osteochondrogenic cluster was markedly expanded in *Txnip*$^{-/-}$ mice. The pathway analysis of the VSMC-derived cells revealed enrichment of bone- and cartilage-formation–related pathways and bone morphogenetic protein signaling in *Txnip*$^{-/-}$ mice. Reanalyzing public single-cell RNA-sequencing dataset revealed that TXNIP was downregulated in the modulated VSMC and osteochondrogenic clusters of human calcified atherosclerotic lesions. *Tagln*-Cre; *Txnip*$^{flox/flox}$ mice recapitulated the calcification and collagen-rich atherosclerotic phenotypes of *Txnip*$^{-/-}$ mice, whereas the hematopoietic deficiency of TXNIP did not affect the lesion phenotype. Suppression of TXNIP in cultured VSMCs accelerates osteodifferentiation and upregulates bone morphogenetic protein signaling. Treatment with the bone morphogenetic protein signaling inhibitor K02288 abrogated the effect of TXNIP suppression on osteodifferentiation.

CONCLUSIONS: Our results suggest that TXNIP is a novel regulator of atherosclerotic calcification by suppressing bone morphogenetic protein signaling to inhibit the transition of VSMCs toward an osteochondrogenic phenotype.

GRAPHIC ABSTRACT: A graphic abstract is available for this article.

Key Words: atherosclerosis ■ calcification ■ osteochondrogenic ■ TXNIP ■ vascular smooth muscle cell

Meet the First Author, see p 4

Atherosclerosis currently accounts for most of the worldwide mortality as a major underlying pathological process responsible for serious cardiovascular events (eg, myocardial infarction, heart failure, and stroke).[1,2] During the progression of atherosclerosis, fibrous materials and calcium gradually accumulate in atherosclerotic lesions, which often constitute the majority of plaque components. In particular,

Correspondence to: Jae-Hoon Choi, DVM, PhD, Department of Life Science, College of Natural Sciences, Research Institute of Natural Sciences, Research Institute for Convergence of Basic Sciences, Hanyang Institute of Bioscience and Biotechnology, Hanyang University, Seoul 04763, Korea, Email jchoi75@hanyang.ac.kr or Dae-Yong Kim, DVM, PhD, Department of Veterinary Pathology, College of Veterinary Medicine, Seoul National University, Seoul 08826, Korea, Email daeyong@snu.ac.kr
*S.-H. Woo and D. Kyung contributed equally to this article.
Supplemental Material is available at https://www.ahajournals.org/doi/suppl/10.1161/CIRCRESAHA.122.321538.
For Sources of Funding and Disclosures, see page 69.

Circulation Research is available at www.ahajournals.org/journal/res

Novelty and Significance

What Is Known?

- Vascular smooth muscle cells (VSMCs), a major cellular component of the atherosclerotic aorta, are highly plastic cells that can undergo various phenotypic switches similar to macrophages, mesenchymal stem cells, and osteochondrogenic cells.
- The osteochondrogenic switch of VSMCs is a pivotal cellular process in atherosclerotic calcification.

What New Information Does This Article Contribute?

- Thioredoxin-interacting protein (TXNIP) suppresses atherosclerotic calcification by inhibiting the phenotypic transition of VSMCs toward an osteochondrogenic phenotype.
- The anti-calcification role of TXNIP is mediated by the suppression of BMP (bone morphogenic protein) signaling in the modulated VSMCs, which is a precursor population of osteochondrogenic cells.

Calcification is a characteristic phenomenon of advanced atherosclerotic lesions. Osteochondrogenic cells derived from VSMCs via a phenotypic transition process are major contributors to atherosclerotic calcification. However, the exact molecular mechanism of the osteochondrogenic transition of VSMCs remains to be elucidated. Here, we present TXNIP as a novel critical regulator of atherosclerotic calcification, by inhibiting the phenotypic transition of VSMCs toward an osteochondrogenic phenotype. The anti-calcification effect of TXNIP is mediated by the suppression of both canonical and noncanonical BMP signaling in the modulated VSMCs, which are precursors of osteochondrogenic cells. The effect of TXNIP on VSMCs in the atherosclerotic milieu is considered specific for the transition from the osteochondrogenic phenotype, but other phenotypes are unaltered. These results suggest that TXNIP is a cell-intrinsic checkpoint for the osteochondrogenic response of VSMCs to the atherosclerotic milieu and highlights its importance for plaque calcification.

Nonstandard Abbreviations and Acronyms

BM	bone marrow
BMP	bone morphogenetic protein
DEG	differentially expressed gene
KO	knock out
MAPK	mitogen-activated protein kinase
scRNA-seq	single-cell RNA-sequencing
SMC	smooth muscle cell
TXNIP	thioredoxin-interacting protein
VSMC	vascular smooth muscle cell
WT	wild type

atherosclerotic calcification is a characteristic phenomenon of atherosclerosis. The coronary artery calcium score is highly correlated with the total atherosclerotic plaque burden[3] and can aid in the prediction of patients at high risk for adverse cardiac events.[4] The exact role of atherosclerotic calcification in plaque rupture or stability has not been precisely defined yet; atherosclerotic calcification might have a bidirectional relationship with plaque stability, depending on the size or location of the calcification.[3] In some minor cases, atherosclerotic calcification can lead to thrombosis in the form of a calcified nodule, which is histologically characterized by an erupted calcified mass with a disrupted fibrous cap.[5] Calcified nodules are suspected to be the principal cause of target-lesion revascularization in patients with drug-eluting stents.[6]

Contrary to the previous view of passive and unregulated process, the concept of vascular calcification as an active process recapitulating bone morphogenesis is currently getting attention.[7,8] Several cell types, such as vascular smooth muscle cells (VSMCs), pericytes, and vessel-residing or circulating stem cells, are known to contribute to vascular calcification. These cells acquire an osteochondrogenic phenotype expressing key osteochondrogenic transcription factors, such as RUNX2, SP7, and SOX9, through stimulation by cytokines, such as BMPs (bone morphogenic protein), in combination with various microenvironment factors (eg, inflammation, apoptosis, necrosis, oxidative stress, and mitochondrial dysfunctions).[7]

VSMCs consist of a medial layer of blood vessels that are responsible for maintaining the vascular tone through contractile properties and the production of extracellular matrix.[9] Although most of the vasculature cells originate from the mesoderm, including endothelial cells and various adventitial cells such as fibroblast, immune cells, and resident stem-like cells, arterial VSMCs originate from multiple precursors of different embryonic origins to form highly mosaic-like patterns.[10,11] The ascending aorta, aortic arch, and carotid arteries are derived from the neural crest, whereas the descending aorta and its distal branches derived from somites of the paraxial mesoderm.[11] In addition to its diverse embryonic origin, VSMCs can adopt multiple phenotypes, such as macrophage/

foam cell-like, osteochondrogenic cell-like, mesenchymal stem cell-like, and myofibroblast-like types through a process called phenotypic transition in pathological circumstances, including atherosclerosis.[9] Lineage-tracing studies provided direct evidence that VSMCs are a major source of osteochondrogenic cells in atherosclerotic lesions.[12,13] Moreover, a combination of single-cell RNA-sequencing (scRNA-seq) and a lineage-tracing system directly visualized the process of transitioning VSMCs toward an osteochondrogenic phenotype.[14–16] These studies showed that VSMCs first give rise to intermediate cell (ie, modulated VSMC) cluster expressing gene markers, such as *Ly6a* (*Sca1*), *Lum*, and *Lgals3*, and then transform into osteochondrogenic clusters, which are enriched with bone and cartilage formation and collagen-producing genes.

TXNIP (thioredoxin-interacting protein), or TBP2 (thioredoxin-binding protein 2), initially known as a negative regulator of Trx (thioredoxin), is a member of the α-arrestin protein family containing 2 arrestin-like domains that are responsible for protein–protein interaction. TXNIP is reported to interact with various proteins such as E3 ubiquitin ligase, importin-α, histone deacetylase, Jab1, Mybbp1a, and NLRP3 (NOD-like receptor Protein 3), as well as Trx, implying that TXNIP may act as a scaffolding protein in various signaling pathways.[17] This feature also explains the multifunctional role of TXNIP in various physiological and pathological processes such as proliferation, apoptosis, natural killer cell development, inflammasome activation, fatty acids, and glucose metabolism.[18,19] The genetic ablation of *Txnip* reduced the oxidative inflammatory response in the VSMCs and mitigated the atherosclerotic burden in *ApoE*$^{-/-}$ mice;[20] additionally, human studies have reported a relationship between *TXNIP* polymorphism and hypertension and arterial stiffness.[21,22] Collectively, these studies suggest that TXNIP is deeply involved in the pathophysiological course of the vascular system. Especially, in the public transcriptome database GSE159677, TXNIP was found to be significantly downregulated in the VSMCs of human calcified atherosclerotic lesions.[23] In this regard, we set out experiments to test whether TXNIP has a modulatory role in atherosclerotic calcification. Importantly, the genetic ablation of *Txnip* increased the osteochondrogenic differentiation of VSMCs by enhancing BMP signaling. Thus, we propose TXNIP as a crucial regulator of the osteochondrogenic differentiation of VSMCs in the atherosclerotic milieu.

METHODS

Data Availability

The scRNA-seq data are available in the SRA (Sequence Read Archive) repository under accession number SRA346850. The additional information and study materials related to this study are available from the corresponding authors upon reasonable request.

The detailed methods are provided in the Supplemental Methods section. Please also refer to the Major Resources Table for detailed information regarding the materials and reagents.

RESULTS

Genetic Ablation of *Txnip* in Mice Markedly Increased Atherosclerotic Calcification

We first examined the phenotypical changes in the atherosclerotic lesions of *Txnip* knockout mice (*Txnip*$^{-/-}$; *Txnip* KO). We induced atherosclerosis by the overexpression of gain-of-function PCSK9 mutant using adeno-associated virus with 16 weeks of a high-fat diet (Figure 1A). This method enabled us to avoid time-consuming mouse mating processes, and also provided a proper model for interrogating atherosclerotic calcification, as adeno-associated-virus–mediated PCSK9 overexpression followed by >15 weeks of high-fat diet in C57BL/6 mice is reported to accumulate calcium within the lesion.[24] After having high-fat diet for 16 weeks, all wild type (WT) and *Txnip* KO mice were analyzed of their plasm lipid profiles and the size of atherosclerotic lesions stained by Oil red O (7-μm interval; total, 70–80 serial cryosections) (WT, n = 11; *Txnip* KO, n=8). The atherosclerotic burdens in aortic arch and descending aorta were analyzed by Oil red O staining of en face prepared aortic arch–upper thoracic aorta and serial cryosections (lower thoracic and abdominal) (WT, n=6; *Txnip* KO, n=5). The aortic arch and descending aorta of remaining mice (WT, n=5; *Txnip* KO, n=3) were used for gene expression analysis by quantitative reversed transcriptase polymerase chain reaction (Figure 1A). WT and *Txnip* KO mice showed different lipid profiles (Figure 1B) probably because of the altered liver lipid metabolism in *Txnip* KO mice as previously reported.[25,26] There was no significant difference in body weight between the 2 groups (WT=42.75±4.03 g, *Txnip* KO=39.85±3.97 g, P=0.1382). Throughout the aorta, *Txnip* KO mice showed decreased Oil red O-stained lesion area compared with WT mice (Figure S1A). In the aortic sinus region, both WT and *Txnip* KO mice showed advanced atherosclerotic lesions (eg, fibroatheroma) with calcifications (Figure 1C through 1G). Although there was no significant difference in the lesion size of aortic sinus region between WT and *Txnip* KO mice (Figure 1C), the atherosclerotic lesions of *Txnip* KO mice were observed to have fewer macrophages (Figure 1D). There were no notable differences in the lesional smooth muscle protein 22-α (SM22α)-positive area (Figure 1E), nor necrotic core size between WT and *Txnip* KO mice (Figure 1F). We next quantified the plaque calcification using Alizarin Red staining. Notably, the atherosclerotic lesions of *Txnip* KO mice carried significantly higher

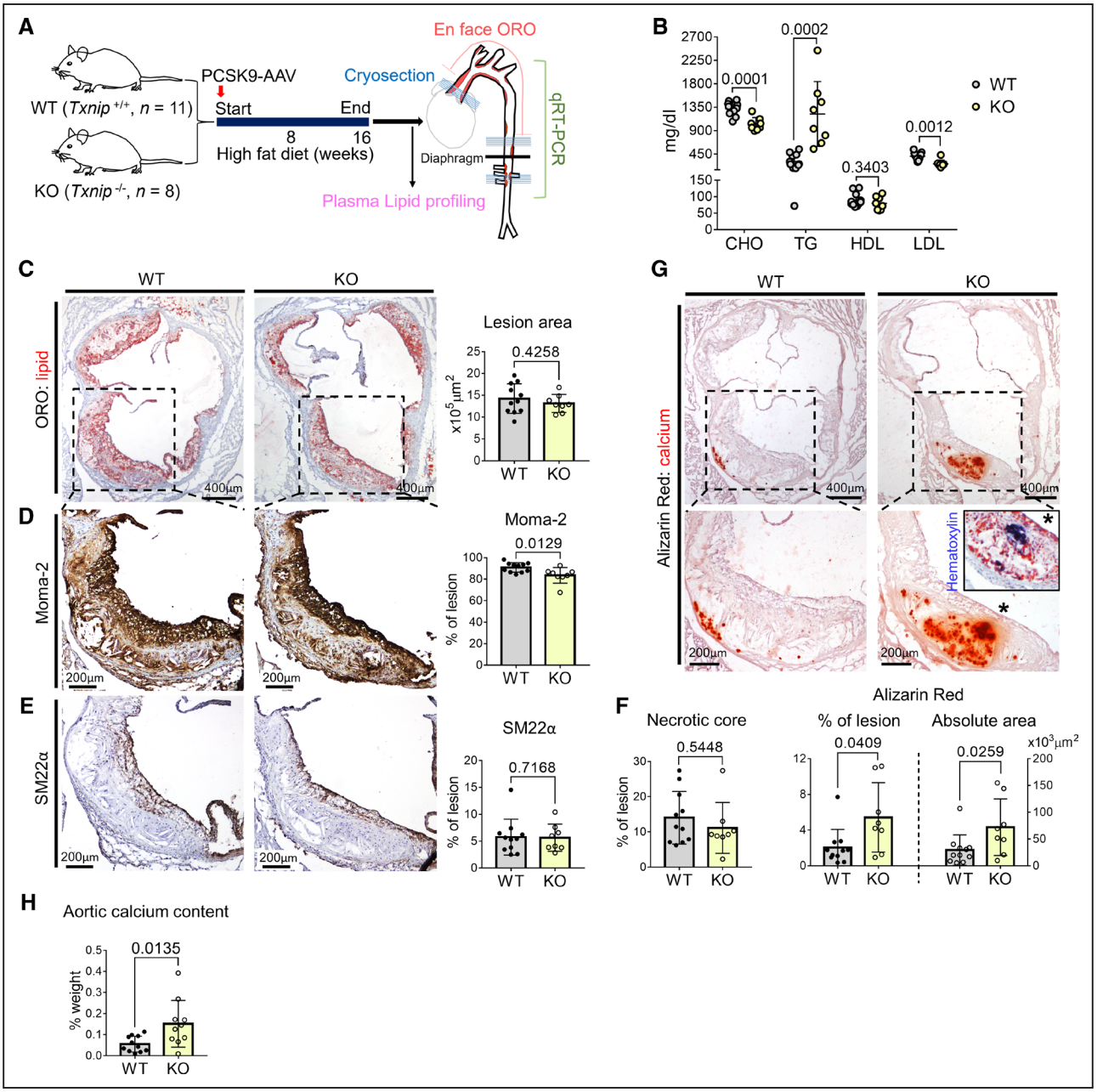

Figure 1. *Txnip* knockout mice (*Txnip* KO) have increased atherosclerotic calcification.
A, Schematic illustration of the experiment. The mice were injected with PCSK9-AAV (adeno-associated virus serotype 8 encoding mouse proprotein convertase subtilisin/kexin type 9) and fed high fat diet (HFD) for 16 weeks. *n*=11/8 for wild type (WT)/*Txnip* KO. **B**, Plasma concentrations of total cholesterol (CHO), triglyceride (TG), high-density lipoprotein (HDL), and low-density lipoprotein (LDL). **C**–**G**, Characterization of atherosclerotic lesions using the 7 μm of perpendicular serial sections (total 70–80 sections) prepared from the aortic sinus. Representative serial sections and quantification results of Oil Red O (ORO) staining (**C**, for lesion size), Moma-2 immunostaining (**D**, for monocyte/macrophage), smooth muscle protein 22-α (SM22α) immunostaining (**E**, for SM22α positive area), necrotic core area (**F**), and Alizarin red staining (**G**, for calcium). **H**, Result of total calcium content measurement. Aortas ranging from the aortic sinus to the aortic arch, which mostly contains advanced plaques expected to be rich in calcification were used. Data are presented as a percentage of dry tissue weight. *n*=11/10 for WT/*Txnip* KO. The applied statistical tests and results are summarized in the Table S11. The error bars denote standard deviation. The exact *P* values are specified. qRT-PCR indicates quantitative reversed transcriptase PCR.

amounts of plaque calcification than those of WT mice, as measured by both the ratio to lesion size and absolute area (Figure 1G). We also measured the total calcium content of the aorta ranging from the aortic sinus to the aortic arch, which mostly contained advanced atherosclerotic plaques that were expected to be rich in calcification. Atherosclerotic aortas of *Txnip* KO mice had a higher calcium content compared with WT mice (Figure 1H). Furthermore, the atherosclerotic lesions of *Txnip* KO mice showed significantly higher expressions

of the bone-related marker gene *Ibsp* (bone sialoprotein) and *Alpl* (alkaline phosphatase) (Figure S1B and S1C). Serum concentrations of Ca^{2+} were similar between WT and *Txnip* KO mice (WT=11.37±0.51 mg/dL, *Txnip* KO=11.26±1.31 mg/dL, *P*=0.7934), indicating the absence of endocrinological effects on calcification-rich phenotype of *Txnip* KO mice.

ScRNA-seq Analysis Revealed that the Osteochondrogenic Cluster Enriched With Bone-, Cartilage-, and Collagen-Related Genes Was Markedly Expanded in *Txnip* KO Mice

To define the cell types responsible for enhanced plaque calcification in *Txnip* KO mice, we performed unbiased cellular characterization of the atherosclerotic aortas of WT and *Txnip* KO mice using scRNA-seq analysis (Figure 2A). The sample preparation procedures for scRNA-seq are shown in Figure S2A. The regions from the aortic sinus to aortic arch were selected for the experiment because majority of these areas contained advanced atherosclerotic plaques that were expected to be rich in calcifications. The adventitia was removed to focus on cell populations within the plaque. The in situ hybridization of *Ly6a* and *Myh11* confirmed the cleanliness of the adventitia, as demonstrated by the absence of adventitial *Ly6a*$^+$ cells (Figure S2B). The enzymatically dissociated atherosclerotic plaque cells from 4 mice for each of the WT and *Txnip* KO groups were pooled and proceeded to FACS live cell sorting (Figure S2C). Through the forward/side scatter parameters and propidium iodide-negative cell selection, 1.35×10^5 and 1.44×10^5 live single cells for WT and *Txnip* KO were obtained and proceeded to gel bead-in-emulsions construction to target a single-cell resolution of ≈10 000 cells. Knee plots were drawn by the default CellRanger count, and 7186 and 11 852 cells for WT and *Txnip* KO, respectively, passed the second knee (Figure S2D). The cells were then filtered out further using mitochondrial gene UMI counts, nFeature, and nCount parameters (Figure S2E and S2F). Finally, a total of 6564 and 11 262 WT and *Txnip* KO cells, respectively, passed quality control and proceeded to the generation of single-cell transcriptome. Before proceeding to the cluster-based analysis, we briefly analyzed the transcriptomes of total cell populations of WT and *Txnip* KO. Among the 24 683 total detected genes, 21 936 genes were commonly expressed in both WT and *Txnip* KO, and 477 differentially expressed genes (DEGs) were observed (Table S1). Notably, gene ontology analysis on the DEGs of whole cells between WT and *Txnip* KO showed the enrichment of bone and cartilage-related pathways in *Txnip* KO (Table S2). Next, we proceeded to cluster-based analysis. The cluster was divided by cutoff with the resolution of the default value $1{\cdot}e^{-4}$ of monocle 3. The scRNA-seq captured most of the typical atherosclerotic lesion cell clusters (Figure 2B). The top 5 DEGs for each cluster are shown by heatmap in Figure 2C, and the top 25 DEGs are listed in Table S3. Gene ontology analysis results using the top 25 DEGs for each cluster justified the cell group annotation (Table S4). In line with previous reports, we identified a VSMC-derived pioneer cluster, which juxtaposed to VSMC cluster known as modulated VSMC, *Ly6a*$^+$ VSMC, or intermediate cell state, which expresses *Ly6a* with decreased contractile genes (Figure 2D).[14,27,28] This cluster also expressed *Lum*, *Fn1*, and *Lgals3* (Figure S3A), sharing the transcriptomic signature of fibromyocyte[15,29] and *Lgals3*$^+$ VSMC.[16] Next, we identified a distinct cluster enriched with both osteogenic transcripts such as *Ibsp*, *Sp7* (osterix), and *Alpl*, and chondrogenic transcript such as *Acan* (aggrecan), *Sox9*, and *Chad* (chondroadherin), together with collagen-producing genes (Figure 2C and 2E; Figure S3B and S3C). We designated this cluster as the osteochondrogenic cluster, which shared transcriptomic features of the previously reported fibrochondrocyte,[14] chondromyocyte,[15] and osteogenic[16] populations.

Ablation of *Txnip* markedly expanded the osteochondrogenic cluster (Figure 2F and 2G), in line with the calcification-rich phenotype observed in *Txnip* KO mice. As the osteochondrogenic cluster highly expressed collagen-producing and cartilage-related genes, we further characterized theses phenotypes on the histological sections from additional atherosclerosis-induced WT and *Txnip* KO mice (Figure 2H through 2J). Indeed, the atherosclerotic lesion of *Txnip* KO mice showed a higher amount of lesional collagen (Figure 2H) and Alcian blue-positive glycosaminoglycans (ie, extracellular matrix of cartilage; Figure 2I). The latter is further supported by the enrichment of chondroitin sulfate biosynthetic-process–related genes (gene ontology ID: 0030206) in the osteochondrogenic cluster (Figure S3D). Next, we performed Masson trichrome staining, Hematoxylin and Eosin staining, and immunostaining of the osteochondrogenic marker ACAN and CHAD proteins in 7 μm of serial cryosections. ACAN and CHAD immunostaining confirmed the transcriptional differences between WT and *Txnip* KO at the protein level (Figure 2J). ACAN and CHAD-positive areas also co-localized with the collagen-rich and calcified areas in the serial sections (Figure 2J).

Hematopoietic Deficiency of TXNIP Did Not Affect Atherosclerotic Calcification

Although VSMCs are known to play a major role in atherosclerotic calcification, immune cells such as macrophages/foam cells can directly affect the calcification via producing matrix vesicles[30] or providing a nucleating site through cell death/apoptosis, and also indirectly by creating a microenvironment facilitating calcification by inflammatory cytokines or secreting BMPs.[7] Accordingly, we tested whether the hematopoietic absence of TXNIP could affect atherosclerosis using a bone marrow (BM) transplantation mouse model. The BM cells of WT

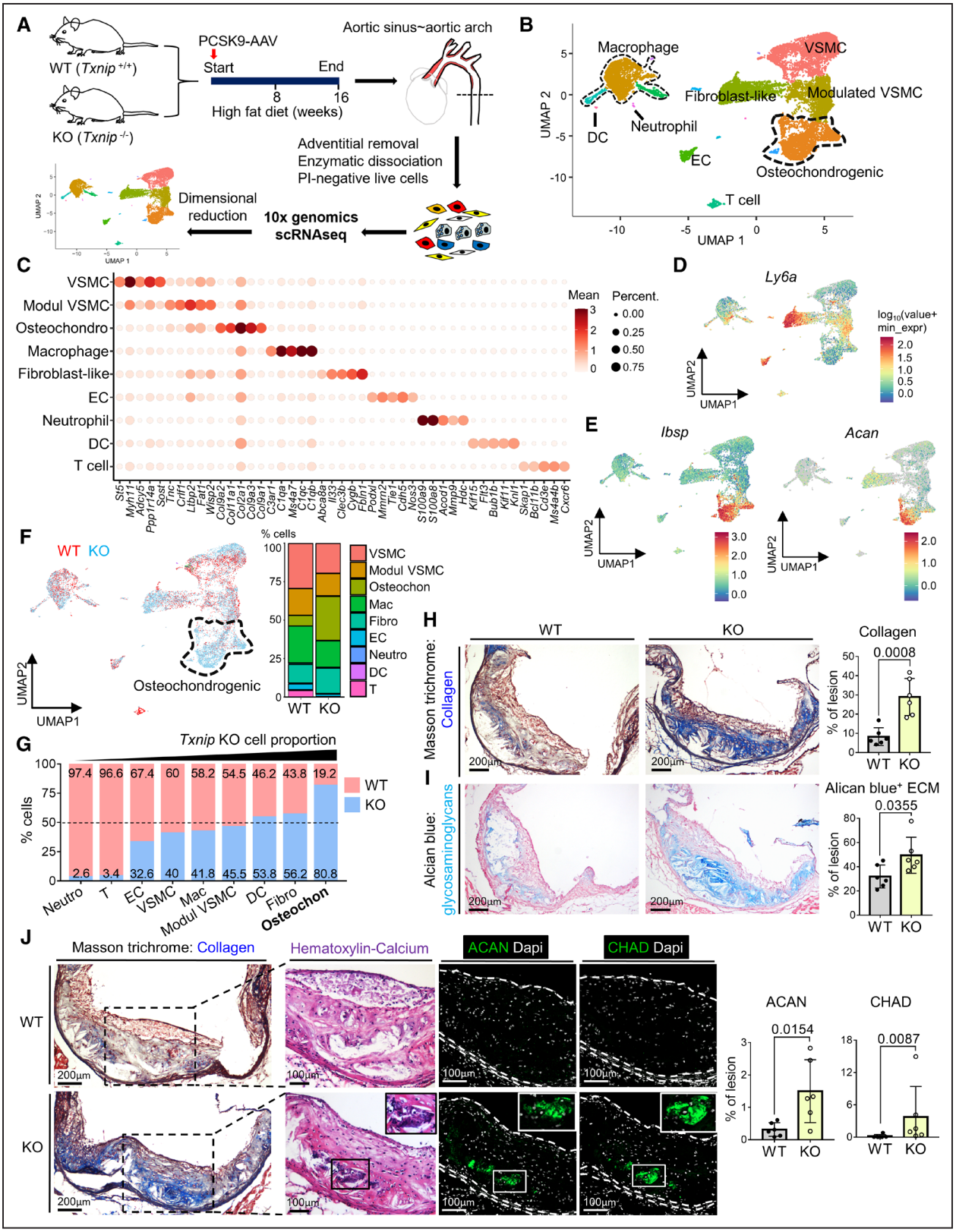

Figure 2. Single-cell RNA-sequencing (scRNA-seq) analysis reveals the osteochondrogenic cluster enriched with bone- and cartilage-related genes, which is markedly expanded in *Txnip* knockout mice (*Txnip* KO) mice.

A, Overall experimental procedure. The atherosclerotic plaques of 4 mice from each wild type (WT) and *Txnip* KO were pooled. After adventitial removal, the atherosclerotic lesion cells were enzymatically dissociated, and propidium iodide (PI)-negative cells were subjected to scRNA-seq. **B**, Uniform manifold approximation and projection (UMAP) visualization of integrated WT and *Txnip* KO scRNA-seq data. **C**, Top 5 differentially expressed genes (DEG) for each cluster. **D** and **E**, Feature plots for *Ly6a*, osteogenic marker *Ibsp*, and chondrogenic marker *Acan* (aggrecan). **F**, UMAP and cluster-annotated bar charts showing distributions of WT and *Txnip* KO cell. (*Continued*)

or *Txnip* KO mice were transplanted into lethally irradiated WT mice (hereafter named BM^{WT} and BM^{KO} mice for each group). After 6 weeks of BM reconstruction, the mice were injected with PCSK9-adeno-associated virus and fed high-fat diet for 16 weeks (Figure 3A). We confirmed the transplantation of WT and *Txnip* KO BM cells by blood PCR (Figure 3B). The lipid profiles of BM^{WT} and BM^{KO} mice were comparable, except for a slight elevation of plasma LDL (low-density lipoprotein) in BM^{KO} mice (Figure 3C). We did not observe any notable differences between the BM^{WT} and BM^{KO} mice in the lesion size, macrophage contents, plaque calcification, collagen content, or Alcian Blue-positive extracellular matrix content (Figure 3D through 3I).

VSMCs Are Primary Source of the Modulated VSMCs and Osteochondrogenic Population

Since we could not trace the VSMC-derived cells using our scRNA-seq data set alone (ie, due to the lack of a smooth muscle cell [SMC]-lineage tracing reporter system), we integrated our data with the data from Pan et al.[14] Pan et al labeled the SMC-lineage cells permanently with ZsGreen1 fluorescence using *Myh11*-$CreER^{T2}$ on *Ldlr* KO background (*ROSA26*$^{ZsGreen1/+}$; *Ldlr*$^{-/-}$; *Myh11*-$CreER^{T2}$). The data from Pan et al consisted of 4 time points (0, 8, 16, and 26 weeks of atherosclerosis induction), and all time points were integrated into our WT and *Txnip* KO scRNA-seq data. The integration of 2 different scRNA-seq datasets successfully retrieved the most typical atherosclerotic lesion clusters (Figure 4A). The top 5 DEGs for each cluster are shown in a heatmap in Figure 4B, and the top 25 DEGs are listed in Table S5. The representative selected marker genes for the VSMC (*Myh11*), modulated VSMC (*Ly6a*) are shown in Figure 4C and 4D. The representative osteogenic marker genes (*Sp7* and *Ibsp*) and chondrogenic marker genes (*Sox9* and *Acan*) are shown in Figure 4E and 4F. When comparing the cluster proportion between each dataset, *Txnip* KO had a higher proportion of osteochondrogenic cluster than that of Pan et al as well as WT, further confirming the phenotype of *Txnip* KO mice (Figure 4G and 4H). When the integrated data were separated according to ZsGreen1 fluorescence, there were few ZsGreen1 negative cells in the modulated VSMCs and osteochondrogenic clusters (Figure 4I). ZsGreen1 positive cells were overlapped with the modulated VSMCs and osteochondrogenic cells of WT and *Txnip* KO, implying that VSMCs are primary source of the modulated VSMCs and osteochondrogenic population (Figure 4I).

Analyzing VSMC-Derived Cell Clusters Revealed the Enhancement of Bone and Cartilage Formation Pathways in *Txnip* KO Mice

We selected the VSMC lineage cells (VSMCs, modulated VSMCs, and osteochondrogenic clusters) for further analysis. The modulated VSMCs (Modul VSMCs) were separated into 2 clusters depending on the *Ly6a* expression level (*Ly6a*^{low} and *Ly6a*^{high} Modul VSMC) (Figure 5A). Osteochondrogenic populations were separated into 3 clusters. The osteochondrogenic cluster (a) occupied a major portion and was contiguous with the *Ly6a*^{high} Modul VSMC cluster (Figure 5A). The top 25 DEGs for each cluster are listed in Table S6, and the top specific genes are shown in the heatmap (Figure S4A). The feature plots for the selected marker genes *Myh11* (VSMC), *Ly6a* (Modul VSMC), and *Ibsp* & *Acan* (osteochondrogenic) are shown in Figure 5B and 5C. Before proceeding to further analyses, we examined the relationship between normal VSMCs (ie, VSMCs from undiseased aorta) and VSMC-derived cells of WT and *Txnip* KO from atherosclerotic lesions. For this, we integrated the scRNA-seq data GSE1179763 of Dobnikar et al,[28] which consisted of normal VSMCs from the aortic arch and distal thoracic aorta into our dataset. The aortic arch and distal thoracic aorta cells were confined to the VSMC cluster, and showed few or no expression of the Modul VSMCs or osteochondrogenic-cluster–related markers (Figure S4B through S4D), confirming that Modul VSMC and the osteochondrogenic cluster were atherosclerosis-related cell populations.

The proportion of *Ly6a*^{high} Modul VSMCs was similar between the WT and *Txnip* KO mice, whereas all 3 osteochondrogenic clusters were markedly increased in the *Txnip* KO mice (Figure 5D and 5E). To localize the modulated VSMCs and confirm the proportional differences between WT and *Txnip* KO, we performed in situ hybridization. The experiment was validated by probing *Polr2a* & *Ppib* (positive control; constitutively expressed genes of mouse) and *DapB* (negative control; constitutively expressed genes of *E. coli*) on WT atherosclerotic lesions (Figure S5A). We observed medial cells that gained *Ly6a* expression and lost *Myh11* expression,

Figure 2 Continued. G, The bar graphs showing the proportions of WT and *Txnip* KO for each cluster. **H** and **I**, Representative serial sections and quantification results of Masson trichrome staining (**H**, for collagen), Alcian blue (**I**, for glycosaminoglycan extracellular matrix [ECM]) on the aortic sinus of WT and *Txnip* KO. *n*=6/6 for WT/*Txnip* KO. **J**, Representative serial section images showing the Masson trichrome staining, Hematoxylin and Eosin (H&E) staining, and immunostaining of the ACAN and CHAD (chondroadherin) on the aortic sinus sections of WT and *Txnip* KO. Masson trichrome staining, ACAN, and CHAD immunostainings are sequentially performed on 7 um of serial cryosections. H&E staining was performed on the CHAD-stained slides by removing the coverslips. ACAN and CHAD-positive areas were quantified (*n*=6/6 for WT/*Txnip* KO). The applied statistical tests and results are summarized in the Table S11. The error bars denote standard deviation. The exact *P* values are specified. Dapi indicates 4',6-diamidino-2-phenylindole; DC, dendritic cells; EC, endothelial cells; and Modul VSMC, modulated vascular smooth muscle cells.

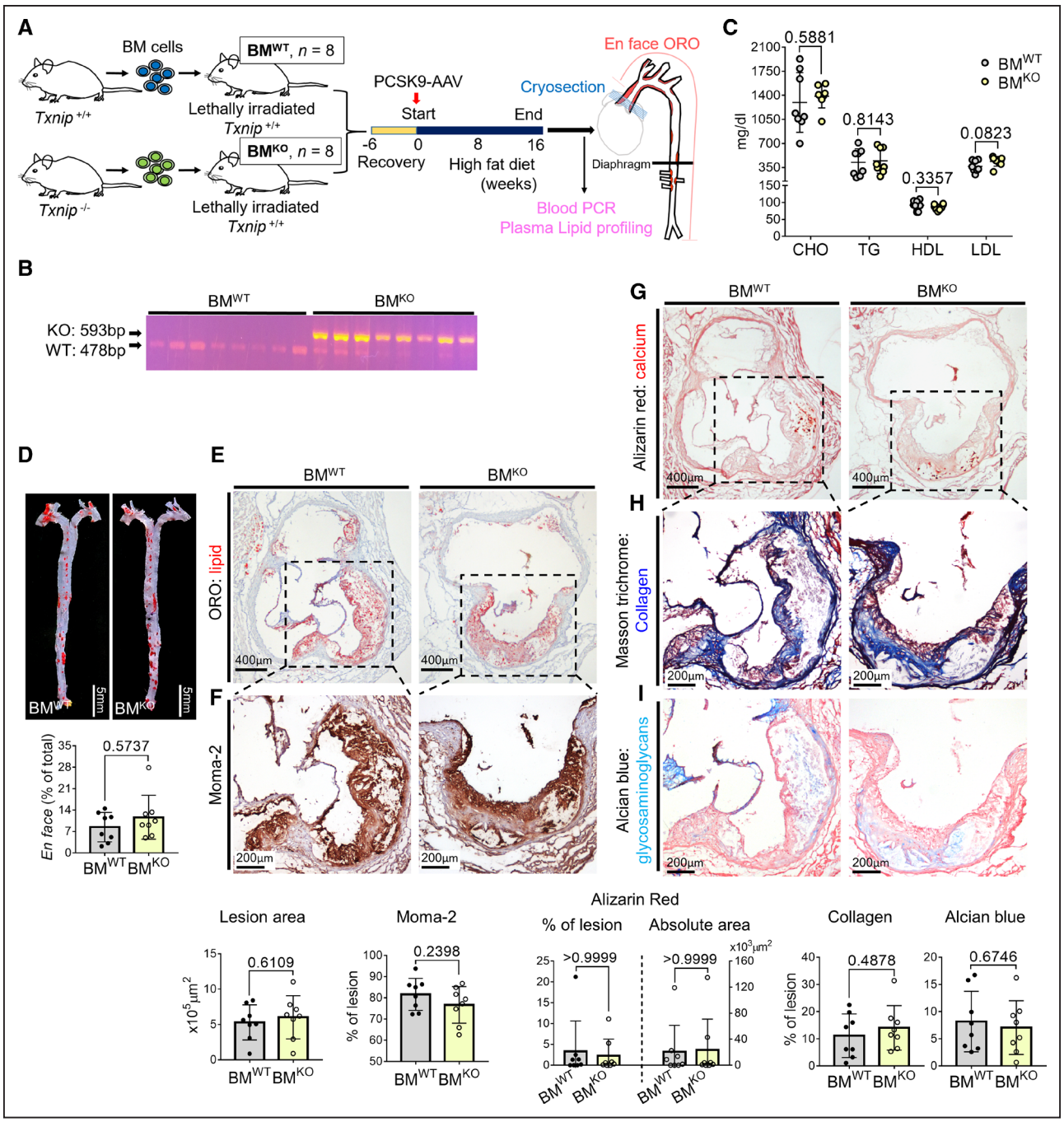

Figure 3. Hematopoietic deficiency of TXNIP (thioredoxin-interacting protein) does not affect the lesion phenotype.
A, Schematic illustration of the experiment. Bone marrow (BM) cells of wild type (*WT*) or *Txnip* knockout mice (*Txnip* KO) were transplanted into WT mice. After 6 weeks of recovery, the mice were injected with PCSK9-AAV and fed HFD for 16 weeks. *n*=8/8 for bone marrow cells of wild type mice (BM^{WT})/ bone marrow cells of Txnip KO mice (BM^{KO}). **B**, Blood PCR result indicating the successful transfusion of the WT and *Txnip* KO BM cells. **C**, The plasma concentrations of total cholesterol (CHO), triglyceride (TG), high-density lipoprotein (HDL), and low-density lipoprotein (LDL). **D**, Comparison of the Oil Red O (ORO)-positive areas between BM^{WT} and BM^{KO} on en-face aorta. **E**–**I**, Characterization of atherosclerotic lesions using the 7 μm of perpendicular serial sections (total 70–80 sections) prepared from the aortic sinus. Representative serial sections and quantification results of Oil Red O (ORO) staining (**E**, for lesion size), Moma-2 immunostaining (**F**, for monocyte/macrophage), Alizarin red staining (**G**, for calcium), Masson trichrome staining (**H**, for collagen), Alcian blue (**I**, for glycosaminoglycan ECM). The applied statistical tests and results are summarized in the Table S11. The error bars denote standard deviation. The exact *P* values are specified.

which represented the cells of the Modul VSMC cluster (Figure S5B). In line with the scRNA-seq data (Figure 5D), WT and *Txnip* KO mice showed comparable medial *Ly6a*$^{+}$*Myh11*$^{+}$ cell numbers (Figure S5B).

To gain insight into the underlying process by which TXNIP regulates atherosclerotic calcification, we first isolated the transcriptome from VSMC, Modul VSMC, and osteochondrogenic clusters (VSMC-derived populations)

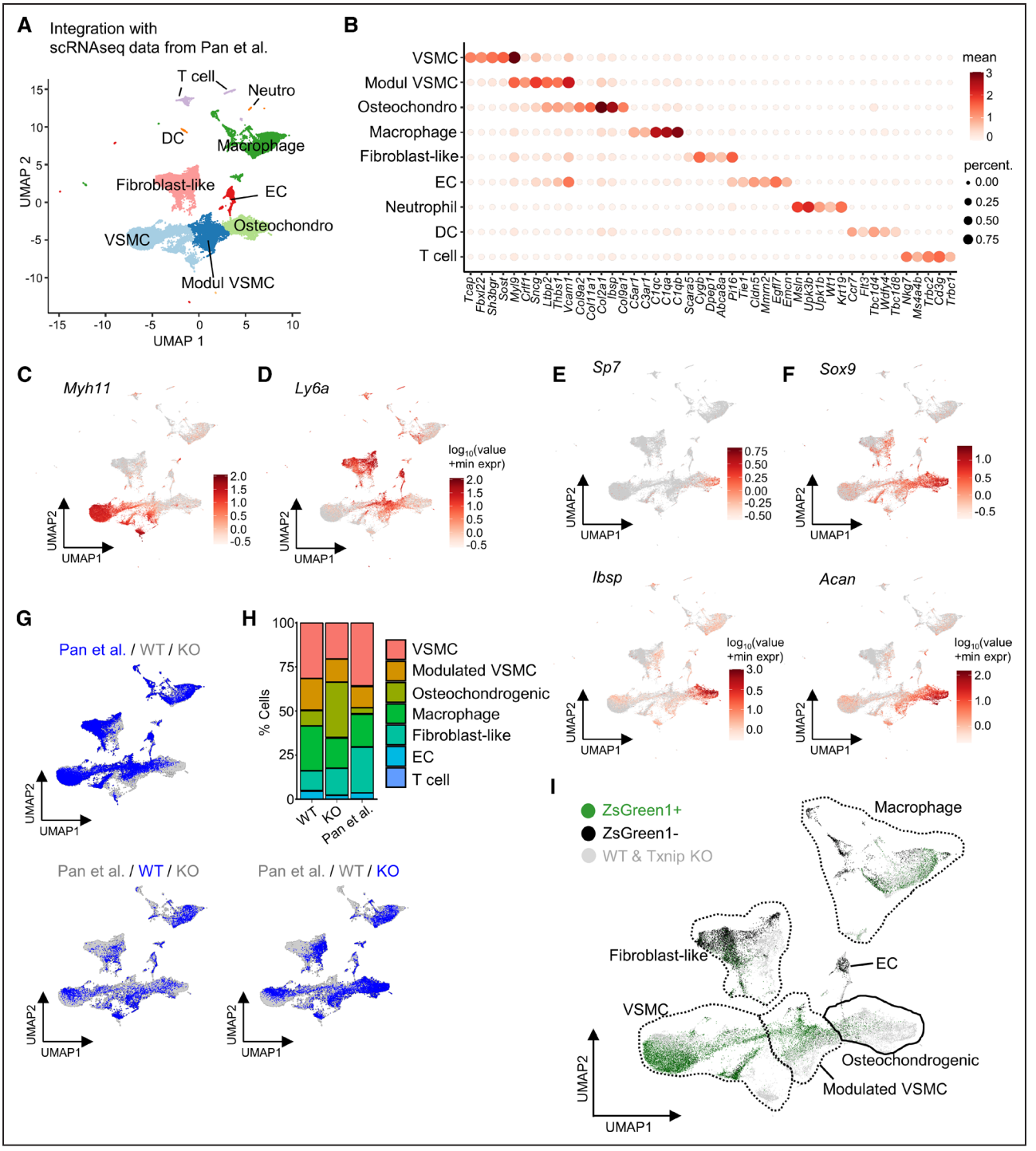

Figure 4. Integration of the single-cell RNA-sequencing (scRNA-seq) data reveals the modulated vascular smooth muscle cell (VSMC) and osteochondrogenic clusters are primarily originated from VSMCs.

Pan et al conducted scRNA-seq of atherosclerotic lesions using ZsGreen1-lineage traced smooth muscle cell (SMC) (*ROSA26*$^{ZsGreen1/+}$; *Ldlr*$^{-/-}$; *Myh11*-CreER^{T2}).[14] **A**, Uniform manifold approximation and projection (UMAP) visualization of 2 integrated scRNA-seq datasets. **B**, Heatmap showing the top 5 differentially expressed genes (DEG) for each cluster. **C** and **D**, Feature plots for *Myh11* and *Ly6a*. **E** and **F**, Feature plots for representative osteogenic genes *Sp7* and *Ibsp*, and chondrogenic genes *Sox9* and *Acan*. **G**, Separate visualization of Pan et al, wild type (WT), and *Txnip* knockout mice (*Txnip* KO) cells on UMAPs. **H**, Bar charts showing proportions of each clusters of Pan et al, WT, and *Txnip* KO. **I**, ZsGreen1 fluorescence-positive and -negative cells are shown on UMAP. DC indicates dendritic cells; and EC, endothelial cells.

and performed a DEGs analysis between the WT and *Txnip* KO. The bone- and cartilage-related genes, such as *Comp* (cartilage oligomeric matrix protein), *Sparc* (secreted protein acidic and cysteine rich), *Hapln1* (hyaluronan and proteoglycan link protein 1), *Ibsp*, *Acan*, and various collagen-producing genes, were highly

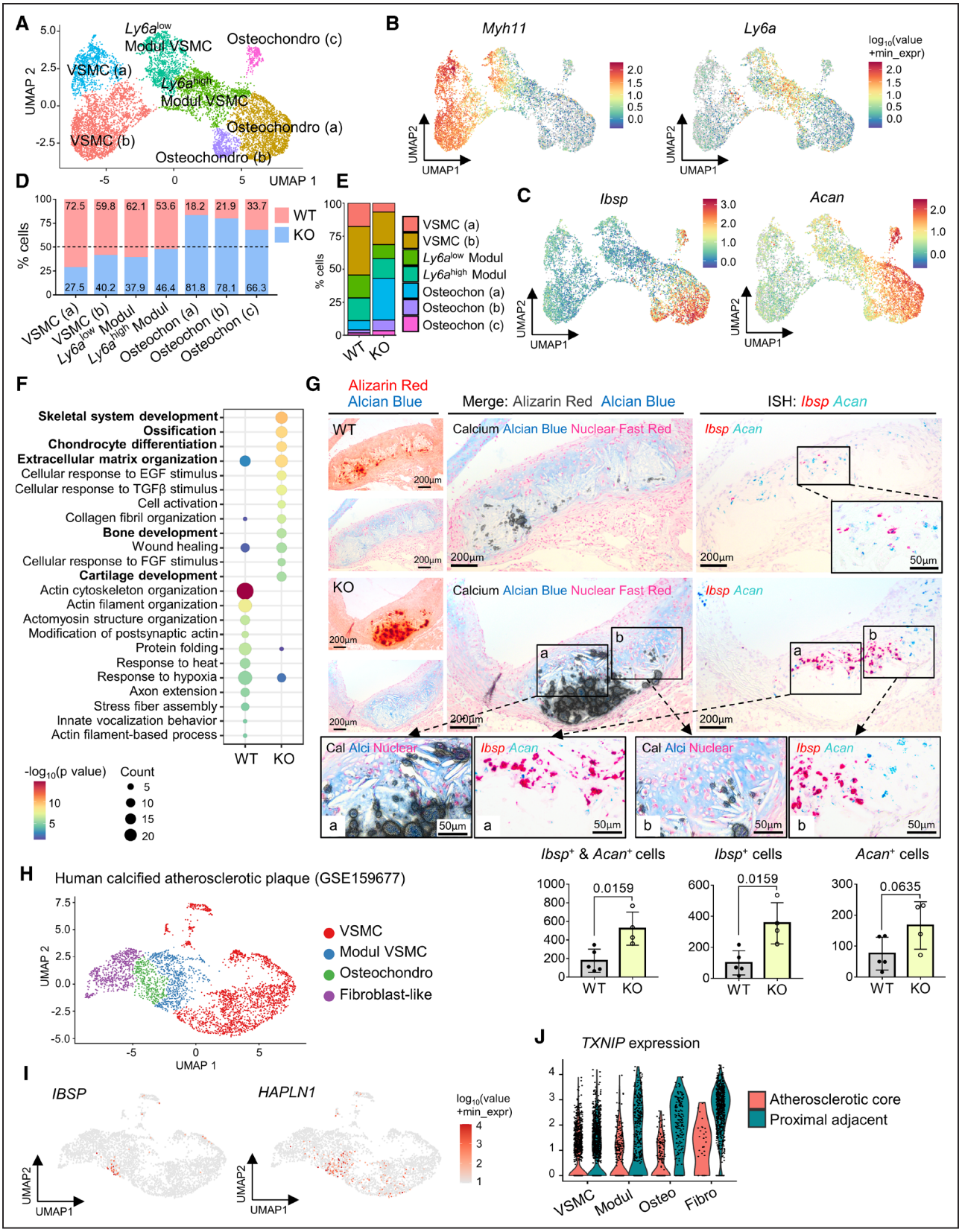

Figure 5. Analyzing vascular smooth muscle cell (VSMC)-derived cell clusters reveals the enhancement of bone and cartilage formation pathways in *Txnip* knockout mice (*Txnip* KO) mice, and the downregulation of *TXNIP* (thioredoxin-interacting protein) in human calcified atherosclerotic plaques.

A, Uniform manifold approximation and projection (UMAP) of sub-clustered VSMC-derived cells. Modul, modulated. **B** and **C**, Feature plots for *Myh11*, *Ly6a*, *Ibsp*, and *Acan*. **D** and **E**, Bar graphs showing the proportions of wild type (WT) and *Txnip* KO mice for each cluster. (*Continued*)

upregulated in VSMC-derived cells of *Txnip* KO (Figure S6; Table S7). Correctly so, *Txnip* occupied the top position of the WT-enriched genes. Next, we performed a gene ontology analysis using the DEGs of VSMC-derived cells of WT and *Txnip* KO. The pathways, such as skeletal system development, ossification, chondrocyte differentiation, extracellular matrix organization, bone development, and cartilage development were enriched in the VSMC-derived cells of *Txnip* KO (Figure 5F).

Characterization of Osteogenic and Chondrogenic Populations

In normal skeletal development, osteoblasts can either be directly differentiated from mesenchymal stem cells (intramembranous ossification) or sequentially differentiated via cartilage templates provided by chondrocytes (endochondral ossification).[31] Although osteogenic and chondrogenic cells can share the same ancestors (eg, mesenchymal stem cells and osteochondrogenic progenitor cells), they eventually differentiated into functionally distinct populations.[31,32] Therefore, we attempted to determine whether the osteochondrogenic populations in the scRNA-seq data could be further divided into osteogenic and chondrogenic populations. Haseeb et al. performed scRNA-seq using mouse femoral and tibial epiphyses, which contain articular cartilage and growth plates,[33] and provided excellent reference markers for osteogenic (*Sp7*, *Ibsp*, *Bglap*) and chondrogenic (*Sox9*, *Acan*, *Matn3*) cells in the normal skeleton. Although there were some differences among the subclusters, both osteogenic and chondrogenic markers are expressed in the osteochondrogenic (a), (b), and (c) clusters (Figure 5C; Figure S7A through S7C). Gene ontology analysis using the DEGs also showed the dual enrichment of the bone and cartilage-related pathways in the osteochondrogenic (a) and (c) clusters (Table S8). In the case of the osteochondrogenic cluster (b), it highly expressed *Spp1* gene and showed enrichment of metal-ion homeostasis and immune response pathways (Figure S7C; Table S8). Overall, we cannot accurately classify the osteochondrogenic clusters into the osteogenic and chondrogenic populations based on the scRNA-seq data alone.

Next, we attempted to comprehensively characterize the relationships between calcification, cartilage metaplasia, and osteogenic and chondrogenic populations. For this, Alizarin Red and Alcian Blue staining were sequentially performed on the same sections (see Supplemental Method), and double in situ hybridizations of *Ibsp* and *Acan* were performed on the 3 μm- adjacent serial sections (Figure 5G; Figure S8). We observed both mixed and locally distinct distribution patterns of calcification and cartilage metaplasia areas (lacunae-shaped cells with Alcian Blue$^+$ extracellular matrix) (Figure 5G; Figure S8). The latter pattern was more prominent as the calcified foci increased, showing a sheet-like pattern. In line with the scRNA-seq data, cells expressing either *Ibsp* or *Acan*, which represents the osteochondrogenic cluster, were significantly more abundant in *Txnip* KO mice (Figure 5G). Among the *Ibsp*$^+$ and *Acan*$^+$ cells, the *Ibsp*$^+$ cells showed a more pronounced increment in *Txnip* KO mice. Next, we examined the expression patterns of *Ibsp*$^+$*Acan*$^-$ (representing the normal osteogenic cells), *Ibsp*$^-$*Acan*$^+$ (representing the normal chondrogenic cells), and *Ibsp*$^+$*Acan*$^+$ cells. Overall, there were few *Ibsp*$^+$*Acan*$^+$ cells found in the in situ hybridization results (Figure S8B and S8C). In the proximity of the calcified area, *Ibsp*$^+$*Acan*$^-$ cells were mostly observed over *Ibsp*$^-$*Acan*$^+$ cells in both WT and *Txnip* KO (*Ibsp*$^+$*Acan*$^-$ cells=83.44±5.33% and 89.15±6.34% for WT and *Txnip* KO; Figure S8B). In the cartilage metaplasia area, *Ibsp*$^-$*Acan*$^+$ cells were primarily observed (67.76±21.93%), although a proportion of *Ibsp*$^+$*Acan*$^-$ cells were also observed (27.31±18.43%) in the case of WT mice (Figure S8C). *Txnip* KO mice showed an increased proportion of *Ibsp*$^+$*Acan*$^-$ cells (43.23±16.75%) in the cartilage metaplasia area (Figure S8C). We speculate, therefore, that *Ibsp*$^+$*Acan*$^-$ cells in the cartilage metaplasia area might represent the cells undergoing endochondral ossification,[34] or may represent abnormal chondrogenic differentiation in the atherosclerotic milieu.

TXNIP Is Downregulated in the Modulated VSMCs and Osteochondrogenic Cells of Human Calcified Atherosclerotic Plaques

In order to determine the relevance of the obtained mouse experimental data to human diseases, we first determined whether modulated VSMC and osteochondrogenic populations exist in human atherosclerotic lesions. To this end, we obtained VSMCs and fibroblast-like cells from scRNA-seq data from a total of 48 patient samples across 4 previous studies (GSE155512,[14] *n*=3; GSE159677,[23] *n*=3;

Figure 5 Continued. F, Results of gene ontology pathway analysis using differentially expressed genes (DEG) of VSMC-derived cells from WT and *Txnip* KO.**G**, Characterizing osteogenic and chondrogenic populations. Alizarin Red and Alcian Blue staining were sequentially performed on the same sections (see Supplemental Methods). Double in situ hybridizations of *Ibsp* and *Acan* were performed on the 3-μm adjacent serial sections. Alizarin Red signals were converted to grayish-scale and superimposed on the Alcian Blue sections using Photoshop software (see Supplemental Methods). *n*=5/4 for WT/*Txnip* KO. **H**–**J**, Downregulation of *TXNIP* in the modulated VSMCs and osteochondrogenic cells of human calcified atherosclerotic plaques. Alsaigh et al (GSE159677) conducted single-cell RNA-sequencing (scRNA-seq) on the atherosclerotic core portion (AC) of endarterectomized type VII calcified plaques matched with the proximal adjacent regions (PA).[21] VSMC cluster (*MYH11* and *ACTA2* positive cluster) of GSE159677 was reanalyzed. **H**, UMAP showing reprocessed VSMC cluster. **I**, Feature plots for *IBSP* (osteogenic) and *HAPLN1* (chondrogenic). **J**, Violin plots showing the expressions of *TXNIP*. The applied statistical tests and results are summarized in the Table S11. The error bars denote standard deviation. The exact *P* values are specified. EGF indicates epidermal growth factor; FGF, fibroblast growth factor; ISH, in situ hybridization; Modul, modulated; and TGFβ, transforming growth factor β.

GSE131780,[29] *n*=4; Slenders et al,[35] *n*=38) and then integrated them with WT mice scRNA-seq data (Figure S9A through S9H). Joint clustering showed that, in accordance with previous reports,[14–16] both modulated VSMC (cluster 0) and osteochondrogenic populations (cluster 6) also exist in human atherosclerotic lesions (Figure S9D). We further confirmed the existence of *IBSP*$^{+}$ and *HAPLN1*$^{+}$ cells in human atherosclerotic lesions, using in situ hybridization (Figure S9I). The *IBSP*$^{+}$ and *HAPLN1*$^{+}$ cells were mostly observed within the lesion. In addition, *IBSP*$^{+}$ cells were frequently localized in proximity to the calcified areas (Figure S9I).

Next, we examined the expressions of TXNIP in the VSMCs of calcified atherosclerotic plaques in humans by reanalyzing the public transcriptome database. Alsaigh et al (GSE159677) conducted scRNA-seq on the atherosclerotic core portion of endarterectomized type VII calcified plaques matched with the proximal adjacent regions.[23]. Reanalyzing the VSMC cluster (*MYH11* and *ACTA2* positive cluster) of GSE159677 gave 4 clusters: VSMC, modulated VSMC, osteochondrogenic and fibroblast-like cluster (Figure 5H). The feature plots for *IBSP* and *HAPLN1* are shown in Figure 5I. *TXNIP* was downregulated in the modulated VSMC (2.87-fold, adjusted *P* value=9.53×10^{-5}), and the osteochondrogenic cluster (4.35 fold, adjusted *P* value=4.57×10^{-21}) of atherosclerotic core compared with proximal adjacent regions (Figure 5J). Subsequently, we observed the expression of TXNIP at the protein level in the human endarterctomized atheroma plaque samples harboring calcification by using immunohistochemistry. TXNIP was diminished in the medial side (marked by α-SMA on the serial sections) of the periphery of the calcified area (Figure S10).

Tagln-Cre; *Txnip*$^{flox/flox}$ Mice Recapitulates the Calcification and Collagen-Rich Plaque Phenotype of *Txnip* KO Mice

To investigate the inhibitory role of TXNIP in atherosclerotic calcification via VSMCs, we generated mice in which *Txnip* was conditionally ablated in SMCs by crossing *Tagln*-Cre and *Txnip*$^{flox/flox}$ mice. *Tagln*-Cre; *Txnip*$^{flox/flox}$ (hereafter named SMC^{KO} mice) and their littermate controls that did not carry the *Tagln*-Cre transgene (hereafter named SMC^{WT} mice) were used. Atherosclerosis was also induced by adeno-associated-virus–mediated PCSK9 overexpression with 16 weeks of high-fat diet (Figure 6A). We analyzed the efficiency and specificity of *Txnip* ablation under the *Tagln* (SM22α) promoter. SMC^{KO} mice showed ≈90% decreased *Txnip* mRNA expression in the aortic media, whereas the expression of liver and quadriceps muscles was comparable to that in SMC^{WT} mice (Figure 6B). In addition, SMC^{KO} showed ≈84% decreased *Txnip* mRNA expression in the adventitia, probably because the *Tagln*-Cre mice used in our experiment (B6.Cg-Tg(Tagln-Cre)1Her/J) also showed Cre expression in perivascular adipocytes and their precursors.[36] TXNIP was successfully eliminated in the SMCs of the aortic media at the protein level in SMC^{KO} mice, whereas the skeletal muscle showed comparable TXNIP level between SMC^{WT} and SMC^{KO} mice (Figure 6C). The lipid profiles of the SMC^{KO} mice were comparable to those of SMC^{WT} mice (Figure 6D). Unlike *Txnip* KO mice, there were no differences in the lesion size nor macrophage burden between SMC^{WT} and SMC^{KO} mice (Figure 6E through 6G). However, notably, SMC^{KO} mice recapitulated the phenotype of *Txnip* KO mice by showing increased lesion calcification and collagen content, and to a lesser extent, an increased Alcian Blue-positive extracellular matrix content compared with SMC^{WT} mice (Figure 6H through 6J).

TXNIP Suppression in VSMCs Accelerate Osteodifferentiation and Augments BMP Signaling

Considering that only the proportion of osteochondrogenic clusters was significantly increased in *Txnip* KO mice and the modulated VSMCs were comparable to WT control, the effect of TXNIP in inhibiting osteodifferentiation would have been exerted in the modulated VSMCs. We selected the primary cultured VSMCs by means of the proper in vitro model (Figure 7A) because cultured VSMCs are reported to mimic *Ly6a*$^{+}$-modulated VSMCs.[28] We verified this finding by examining the expressions of *Ly6a* and *Lum* (upregulated in the modulated VSMC cluster), and the *Myh11* (contractile gene; VSMC marker) along the culture passages. Once (P1) or twice (P2) passaged VSMCs showed significantly increased expression of *Ly6a* and *Lum*, and decreased expression of *Myh11* compared with the initial passage (P0) (Figure 7B). P3 to P4 passaged VSMCs were then treated with negative control siRNA (NC) or *Txnip* siRNA (si-*Txnip*) and subjected to osteodifferentiation (Figure 7A). Western blotting confirmed >90% knockdown of TXNIP in protein level by *Txnip* siRNA (Figure 7C). The suppression of TXNIP significantly accelerated the osteodifferentiation (Figure 7D). We also confirmed the same phenotype in cultured VSMCs from SMC^{WT} and SMC^{KO} (Figure S11A and S11B). Upon osteodifferentiation, TXNIP suppression significantly increased the expression of the key osteogenic transcription factor *Sp7* and the osteochondrogenic cluster-specific genes *Bglap* (osteocalcin) and *Ibsp*. In addition, this resulted in conversely decreased *Myh11* expression (Figure 7E).

Oxidative stress is one of the factors that promote osteocytic phenotype of VSMCs.[8] Because TXNIP is a negative regulator of redox-regulating molecule Trx,[17] the ablation of TXNIP would attenuate VSMC calcification by reducing oxidative stress. However, since we observed the opposite phenotype (ie, ablation/suppression of TXNIP in VSMCs accelerate osteodifferentiation), it appears that another mechanism would play a role in the effect of TXNIP on the osteodifferentiation of

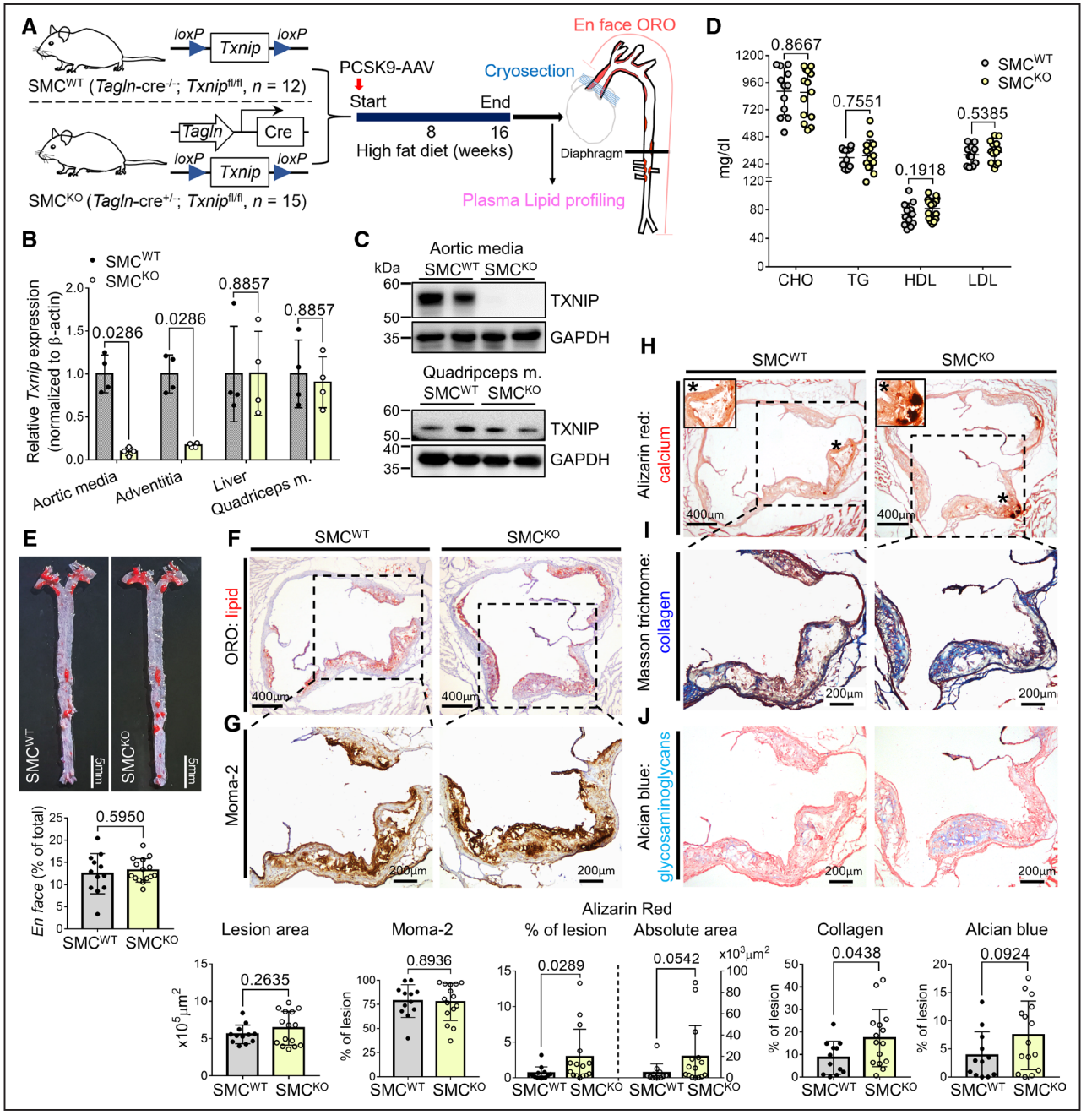

Figure 6. Vascular smooth muscle cell (VSMC)-specific *Txnip* (thioredoxin-interacting protein) ablation recapitulates the calcification-rich plaque phenotype of whole-body *Txnip* knockout mice (*Txnip* KO) mice.

A, Schematic illustration of the experiment. *Tagln*-cre; *Txnip*$^{flox/flox}$ (SMC^{KO}) mice and their littermate controls that did not have *Tagln*-cre (SMC^{WT}) were subjected to atherosclerosis. The mice were injected with PCSK9-AAV (adeno-associated virus serotype 8 encoding mouse proprotein convertase subtilisin/kexin type 9) and fed high fat diet (HFD) for 16 weeks. *n* of SMC^{WT}/SMC^{KO} mice=12/15. **B** and **C**, Validation of SMC-specific ablation of *Txnip*. **B**, qRT-PCR data showing *Txnip* mRNA expression in the aortic media, adventitia, liver, and quadriceps muscle (*n*=4 mice for both groups). *Txnip* expression was normalized to that of *β-actin*. **C**, Western blot showing TXNIP level in the aortic media and quadriceps muscle. The representative blot images of 2 mice per group (a total of 4 mice per group were analyzed). **D**, The plasma concentrations of the total cholesterol (CHO), triglyceride (TG), high-density lipoprotein (HDL), and low-density lipoprotein (LDL). **E**, Comparison of the Oil Red O (ORO)-positive areas between SMC^{WT} and SMC^{KO} on en-face aorta. **F**–**J**, Characterization of atherosclerotic lesions using the 7 μm of perpendicular serial sections (total 70–80 sections) prepared from the aortic sinus. Representative serial sections and quantification results of ORO staining (**F**, for lesion size), Moma-2 immunostaining (**G**, for monocyte/macrophage), Alizarin red staining (**H**, for calcium), Masson trichrome staining (**I**, for collagen), Alcian Blue (**J**, for glycosaminoglycan ECM). The applied statistical tests and results are summarized in the Table S11. The error bars denote standard deviation. The exact *P* values are specified.

VSMCs. BMP signaling plays a pivotal role in bone and cartilage development,[37] and is also known to be deeply involved in the osteodifferentiation of VSMCs in the setting of atherosclerosis.[7,8] In atherosclerosis, BMP2 and BMP4 are known to induce osteodifferentiation, and are expressed in various cell types, such as endothelial

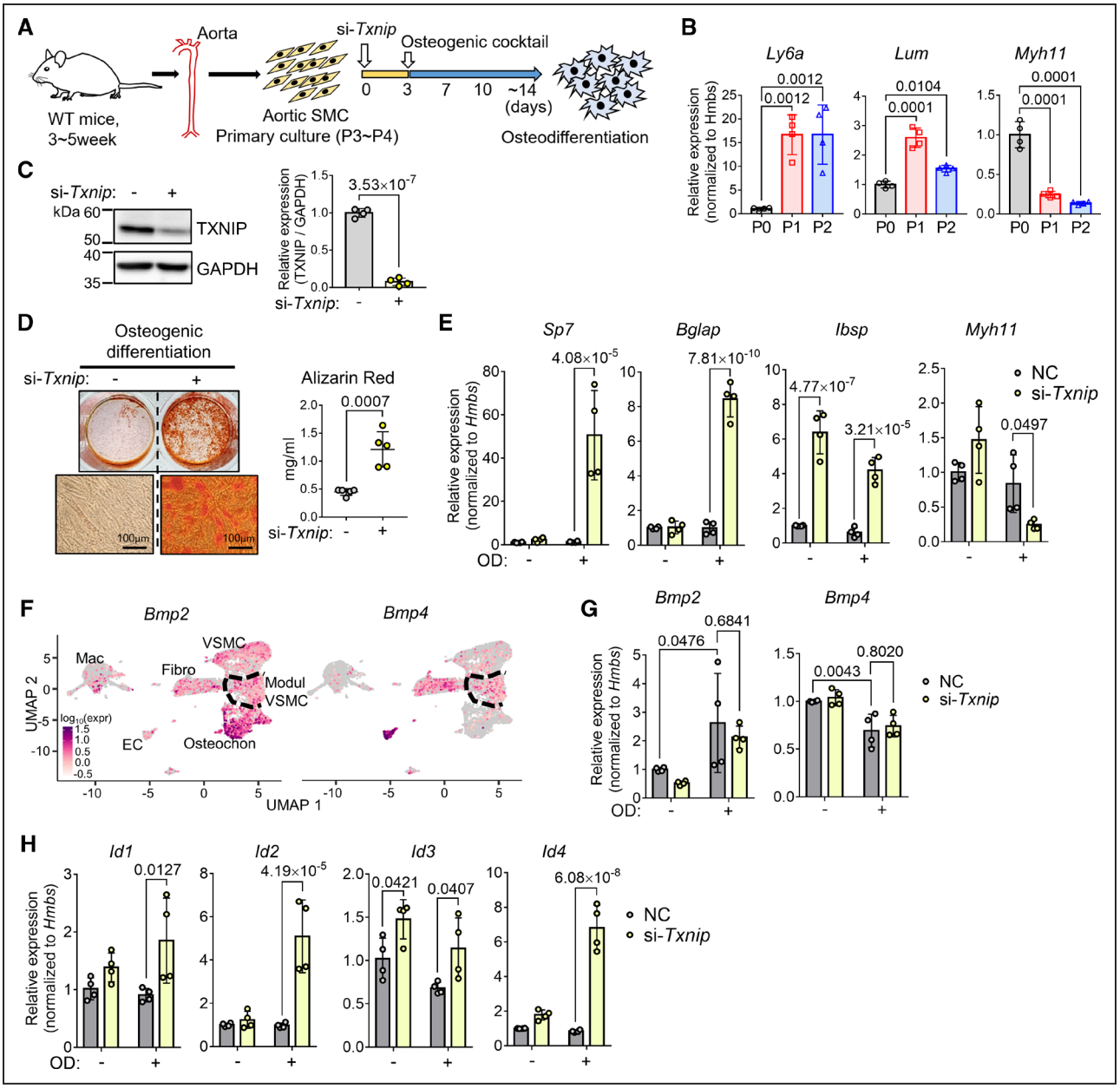

Figure 7. *Txnip* (thioredoxin-interacting protein) knockdown in vascular smooth muscle cells (VSMC) accelerates osteodifferentiation and augments BMP (bone morphogenetic protein) signaling.

A, Schematic illustration of the experiment. The pooled VSMCs from 2 to 3 wild type (WT) mice constituted 1 biological replicate. Cultured VSMCs were treated with negative control (NC) siRNA or *Txnip* siRNA (si-*Txnip*) and were subjected to osteodifferentiation by *osteogenic cocktail* (β-glycerophosphate, L-ascorbic acid, and H_2O_2) incubation. **B**, qRT-PCR results showing the changes in gene expressions of *Ly6a* and *Lum* (upregulated in the modulated VSMC cluster), and the *Myh11* (contractile gene; VSMC marker) along the culture passages. *n*=4. **C**, Western blot confirming knockdown of TXNIP by si-*Txnip*. TXNIP expression was normalized to glyceraldehyde 3-phosphate dehydrogenase (GAPDH) for quantification. *n*=4. **D**, Alizarin Red staining results of osteodifferentiation (end point). The staining was quantified by cetylpyridinium chloride extraction. *n*=5. **E**, qRT-PCR results showing the expressions of *Sp7*, *Bglap*, *Ibsp* (which are the osteochondrogenic marker genes), and *Myh11* (which is a contractile gene; VSMC marker) in the NC and si-*Txnip* treated VSMCs with or without osteodifferentiation. *n*=4. **F**, Feature plots showing *Bmp2* and *Bmp4* expression in WT and *Txnip* knockout mice (*Txnip* KO) single-cell RNA-sequencing (scRNA-seq) data. **G**, qRT-PCR results showing the expressions of *Bmp2* and *Bmp4* in the NC and si-*Txnip* treated VSMCs with or without osteodifferentiation. *n*=4. **H**, qRT-PCR results showing the mRNA expressions of inhibitor of DNA binding (Id) proteins, which are transcribed by BMP as a crucial target of BMP signaling. *n*=4. **E**, **G**, and **H**, *Hmbs* was used as a housekeeping gene for qRT-PCR. The applied statistical tests and results are summarized in Table S11. The error bars denote standard deviation. The exact *P* values are specified. EC indicates endothelial cell; Fibro, fibroblast-like; Mac, macrophage; Modul, modulated; OD, osteodifferentiation; Osteochon, osteochondrogenic; and P, passage.

cells, foam cells, and VSMCs.[7] Indeed, *Bmp2* and *Bmp4* were transcriptionally expressed in almost all the cell types (Figure 7F). Notably, the osteochondrogenic cluster showed higher expression of *Bmp2*, suggesting to the possible self-reinforcement of the osteochondrogenic population. Upon osteodifferentiation, we verified

the expressions of *Bmp2* and *Bmp4* in cultured VSMCs. In line with the scRNA-seq data, the osteodifferentiation increased *Bmp2* but decreased *Bmp4* expression in cultured VSMCs (Figure 7G). Next, we examined the expressions of the inhibitor of DNA binding (Id) proteins, which are transcribed by BMP as a crucial target of BMP signaling.[38] After osteodifferentiation, TXNIP suppression increased the expressions of all classes of Ids (Id1–4), implying up-regulation of BMP signaling by TXNIP suppression (Figure 7H).

TXNIP Inhibits Osteodifferentiation of VSMCs by Suppressing Both Canonical and Noncanonical BMP Signaling

The BMPs transduce their signaling through Smads-involved canonical pathways and p38 mitogen-activated protein kinase (MAPK)-involved noncanonical pathways. In the canonical pathways, the BMP receptors phosphorylate Smad1/5/9 (receptor-activated Smads [R-Smads]), and subsequently translocate into the nucleus in interaction with Smad4 (common Smad [Co-Smad]) to activate the osteogenic program.[37] We examined both canonical and noncanonical BMP signaling under BMP2 stimulation (Figure 8A). TXNIP suppression increased the p-Smad1/5/9 levels and increased the total amount of Smad1 and Smad5. When the inhibitory Smads (i-Smads; Smad6 and Smad7) were examined, Smad6 showed comparable level; however, Smad7 was diminished upon TXNIP suppression. Moreover, TXNIP suppression increased p-p38 (Figure 8A), which is a noncanonical pathway that accelerate osteodifferentiation by increasing the expression and activity of osteoblast-specific transcription factors RUNX2, DLX5, or SP7.[39] Next, we compartmentalized the cytoplasmic and nuclear proteins and examined the Smad4. Notably, both nuclear and cytoplasmic fractions of Smad4 were significantly increased upon TXNIP suppression (Figure 8B). We checked the activities of Smad1 and Smad4 regulons which are defined by the interaction between transcription factor and its target (including binding elements), in the VSMC-derived cell populations of WT and *Txnip* KO scRNA-seq data. Target genes of Smad1 and Smad4 regulons were selected from the DoRoTheA program from a previous study (Table S9).[40] Both Smad1 and Smad4 regulon activities were enriched in the ostechondrogenic clusters (Figure 8C and 8D), suggesting that the BMP signaling pathway was upregulated in *Txnip* KO mice. To test whether the augmentation of BMP signaling under TXNIP suppression is necessary and sufficient for accelerated osteodifferentiation, we used the potent BMP signaling inhibitor K02288.[41] K02288 (10 μM) effectively suppressed both canonical and noncanonical BMP signaling, marked by significant decrease of p-Smad1/5/9 and p-p38 levels (Figure 8E). K02288 treatment abrogated the effect of TXNIP suppression on osteodifferentiation (Figure 8F). We then examined the effect of TXNIP on canonical and noncanonical BMP signaling pathways, respectively, by utilizing *Smad4* siRNA for blocking canonical pathway, and *MAPK14* (p38) siRNA for blocking noncanonical pathway. Both *Smad4* siRNA and *MAPK14* siRNA effectively downregulated Smad4 and p38 protein, each (Figure 8G). The effectiveness of both siRNAs was also maintained in combinatorial treatment with *Txnip* siRNA (Figure 8H). *MAPK14* siRNA also reduced the amount of p-p38 (Figure 8H). The individual or dual suppression of Smad4 and p38 effectively abolished the osteodifferentiation effect of *Txnip* siRNA, suggesting that both canonical and noncanonical BMP signaling pathways are required for the suppressive role of TXNIP on osteodifferentiation (Figure 8I and 8J).

Wnt/β-catenin signaling is also reported to be involved in the osteodifferentiation of VSMCs in atherosclerotic calcification.[42] We checked the regulon activity of Wnt/β-catenin (Table S10). However, we did not find a notable difference in the Wnt/β-catenin regulon activity between WT and *Txnip* KO mice (Figure S12E). Also, TXNIP suppression did not alter the nuclear β-catenin levels in cultured VSMCs (Figure S12F), suggesting that Wnt/β-catenin signaling is not involved in the effect of TXNIP on VSMC osteodifferentiation.

DISCUSSION

Recent studies, using a combination of lineage-traced reporter mice with the scRNA-seq technique, showed generally consistent findings with regard to the process of VSMCs transitioning toward osteochondrogenic clusters.[14–16] VSMCs first give rise to the pioneer cell population (showing similar transcriptomic profiles albeit named differently by each group: intermediate cell state,[14] fibromyocyte,[15] or *Lgals3*$^{+}$ VSMC[16] and then transform into the osteochondrogenic population: fibrochondrocyte,[14] chondromyocytes,[15] or osteogenic).[16] In particular, studies from 2 independent groups showed that SMC-specific ablation of *Ahr* or *Klf4* can increase (*Ahr*) or decrease (*Klf4*) the osteochondrogenic population.[15,16] Notably, the SMC-specific ablation of *Ahr* or *Klf4* also altered the lesion size and fibrous cap, and altered the intermediate VSMC clusters in the case of *Klf4*, suggesting that the regulatory function of these genes in SMC transitioning would not be specifically confined to the osteochondrogenic phenotype. To date, the key regulatory factors and underlying mechanisms that govern the osteochondrogenic transition of VSMCs are yet to be elucidated.

Here, we confirmed the existence of a distinct osteochondrogenic population that is responsible for atherosclerotic calcification, and demonstrated that TXNIP is a novel regulator of atherosclerotic calcification by holding transition of the modulatory VSMCs toward the osteochondrogenic cluster through the suppression of BMP signaling. The regulatory role of TXNIP is thought

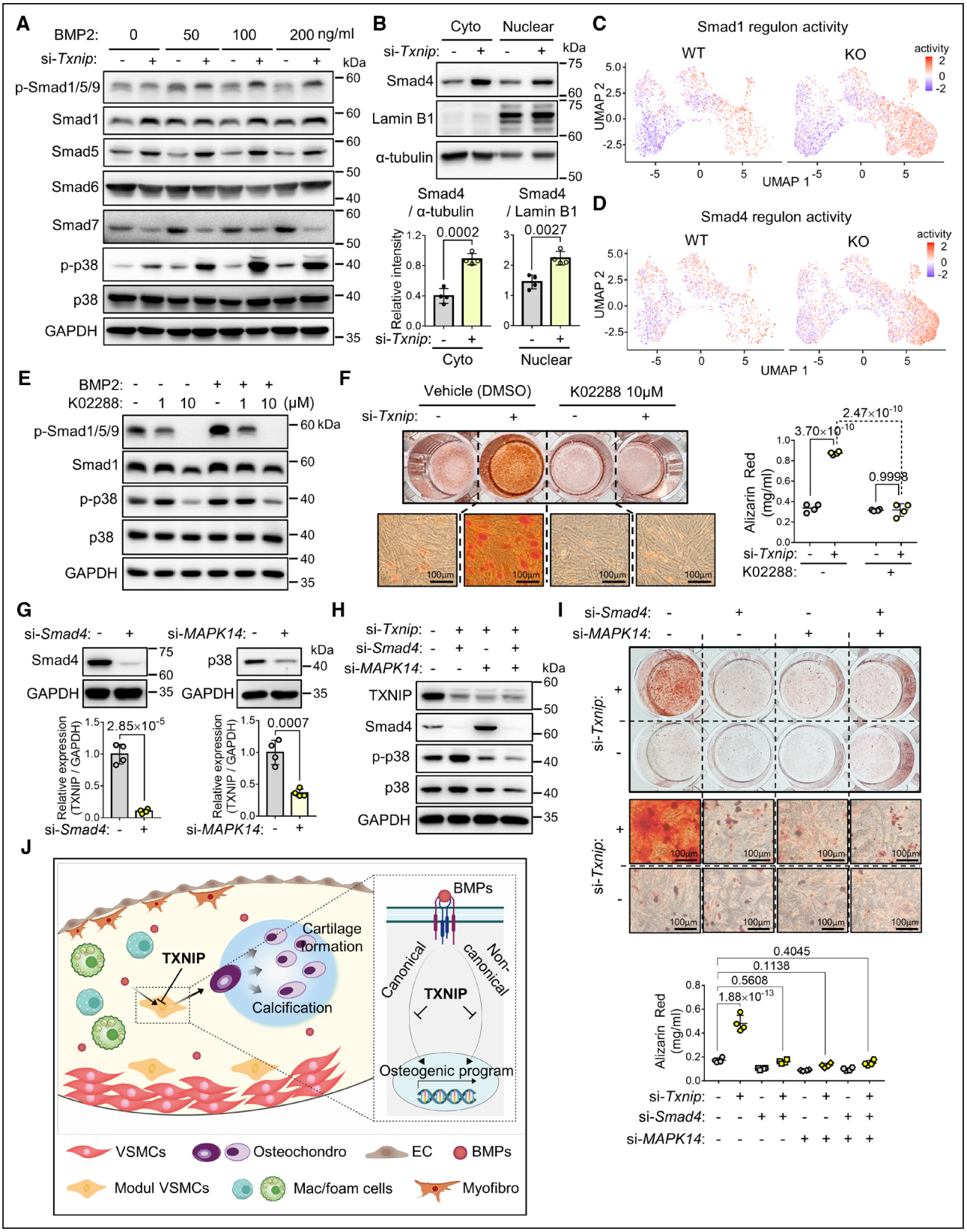

Figure 8. *Txnip* (thioredoxin-interacting protein) knockdown in vascular smooth muscle cells (VSMC) upregulates both canonical and noncanonical BMP (bone morphogenetic protein) signaling leading to osteodifferentiation.

A, Western blot showing canonical and noncanonical BMP signaling upon si-*Txnip* treatment. The results at 16 hours after BMP treatment. The representative images for *n*=4. **B**, Western blot showing cytoplasmic and nuclear fractions of Smad4 upon *Txnip* siRNA treatment. α-tubulin and Lamin B1 were used as the loading controls for the cytoplasmic and nuclear fractions, respectively. *n*=4. (*Continued*)

to be specific to the transitioning process of modulated VSMCs toward osteochondrogenic cells, which is supported by the following data: (1) a comparable proportion of the modulated VSMC cluster in the scRNA-seq, (2) *Ly6a*$^{+}$*Myh11*$^{+}$ cells of in situ hybridization data between WT and *Txnip* KO, and (3) unaltered lesion size and macrophage contents in the SMC^{KO} mice.

In previous studies on AHR and KLF4, the osteochondrogenic cluster was considered a disease-prone cell population, because the amount of osteochondrogenic population was proportional to the lesion size and macrophage content, and inversely proportional to the fibrous cap.[15,16,27] However, *Txnip* KO mice showed markedly expanded osteochondrogenic clusters, but reduced macrophage content and unaltered (in case of the aortic sinus region) or reduced (in case of the aorta) lesion size. Furthermore, *Tagln*-Cre; *Txnip*$^{flox/flox}$ mice showed exclusively increased plaque calcification and collagen content, while other phenotypes remained unchanged. Based on our findings, enhanced lesional calcification in *Txnip* KO mice appears to be caused by osteochondrogenic phenotypic switch of VSMCs regardless of other lesion features including lipid accumulation and macrophage content. For reference, the possible reasons for the altered phenotypes except calcification in *Txnip* KO mice are as follows: (a) results from the different lipid profiles between WT and *Txnip* KO mice; (b) the absence of TXNIP in endothelial cells, as TXNIP is reported to be involved in the regulation of stress fiber formation, inflammatory response, and angiogenesis of endothelial cells.[43–45] The hematopoietic absence of TXNIP was less likely to contribute to the phenotype of *Txnip* KO, as we did not observe any notable differences between BM^{WT} and BM^{KO} mice.

In accordance with previous studies,[14–16] we again confirmed the existence of the modulated VSMCs and osteochondrogenic cells in human atherosclerotic lesions by integrating 4 human scRNA-seq dataset (n=48) with a WT mice dataset. Although we attempted to analyze similarities and/or differences between human and mouse osteochondrogenic clusters, we did not obtain meaningful results. Of note, however, osteochondrogenic cells in the human scRNA-seq data are relatively few in number compared with the WT mice. This might be caused by the underestimation of the number of differentiated osteogenic and chondrogenic cells during scRNA-seq preparation steps,[46] or the chronic nature of human plaques compared with mice plaques, as surgeries tend to be performed after relatively long periods of progression, which can last years. However, this may also simply be a true reflection of the species differences between humans and mice. Unlike mice, chondroid metaplasia in human atheroma is rarely observed,[47] although there have been a few reported cases.[48] Indeed, we did observe *IBSP*$^{+}$ cells in the vicinity of calcification but did not observe cartilage metaplasia areas that co-localized with *HAPLN1*$^{+}$ cells in human sections, as they did in mice (Figure 5G; Figure S8). It is unclear whether these chondrocyte marker-positive cells in human lesions are directly related to cartilage formation or not. The atherosclerotic calcification process in mice that mainly occurs via osteochondrogenic cells may differ, in part, from human processes.[47] Of note, SMC-specific deletion of master osteogenic transcription factor *Runx2* in mice caused 50% to 80% reduction of atherosclerotic calcification.[49,50] This suggest the involvement of mechanisms other than osteochondrogenic transitions of VSMCs, such as the contribution of cell debris originating from apoptotic or necrotic cells, or extracellular vesicles produced by either VSMCs or macrophages.[47] Further studies, such as spatial single-cell analysis, will be required to elucidate the exact relation between the osteochondrogenic cells and atherosclerotic calcification in human lesions.

Here we showed that the suppressive role of TXNIP on VSMC calcification is mediated by BMP signaling. Notably, 2 previous studies showed that TXNIP can aggravate VSMC calcification under certain conditions using in vitro VSMC culture models.[51,52] These studies suggested that ROS and/or autophagy-mediated pathways regarding the augmenting role of TXNIP on VSMC calcification. Indeed, oxidative stress and inflammation are one of the drivers of atherosclerotic calcification,[8] and Byon et al showed that ablation of TXNIP attenuates ROS and inflammatory processes in VSMCs.[20] However, we found that the suppression of TXNIP markedly expanded the osteochondrogenic population, resulting in increased atherosclerotic calcification. This result prompted us to speculate that there should be other mechanism(s) that overturn the above-mentioned effects of TXNIP. We found that the suppression of TXNIP increased both canonical and noncanonical BMP signaling. The suppression of TXNIP increased the activated and total amount of R-Smads (Smad1 and Smad5) and

Figure 8 Continued. C and **D**, Feature plots showing the regulon activities of Smad1 and Smad4 in VSMC-derived cells of wild type (WT) and *Txnip* knockout mice (*Txnip* KO). **E**, Western blot showing the validation result of determining the concentration of the BMP signaling inhibitor K02288. Representative images of *n*=2. **F**, Alizarin Red staining results showing abrogation of the effect of *Txnip* knockdown on osteodifferentiation. In total, 10 μM of K02288 was treated in advance of siRNA transfection, and was added to the osteogenic cocktail for every medium replacement. The staining was quantified by cetylpyridinium chloride extraction. *n*=4. **G**, Western blot confirming knockdown of Smad4 and p38 by si-*Smad4* and si-*MAPK14*, respectively. Expressions were normalized to glyceraldehyde 3-phosphate dehydrogenase (GAPDH) for quantification. *n*=4. **H**, Western blot showing efficacy validation of si-*TXNIP*, si-*Smad4*, and si-*MAPK14* when used in combination, and the reduction of p-p38 by si-*MAPK14*. Representative images of *n*=2. **I**, Alizarin Red staining results showing the abrogation of the effect of *Txnip* knockdown on osteodifferentiation by blocking either the canonical (si-*Smad4*) or noncanonical (si-*MAPK14*) BMP signaling pathway. Cetylpyridinium chloride extraction quantification. *n*=4. The applied statistical tests and results are summarized in Table S11. The error bars denote standard deviation. The exact *P* values are specified.

Co-Smad (Smad4), and decreased Smad7 which is a negative regulator (i-Smad) of TGFβ/BMP signaling.[37,53] In noncanonical signaling, TXNIP suppression increased p38 phosphorylation.

We attempted to further determine the underlying mechanism of how TXNIP regulates BMP signaling. We first checked the mRNA expression levels for Smad1, Smad5, Smad7, and Smad4 molecules, which showed altered proteins level, upon TXNIP suppression (Figure 8A). However, mRNA expressions of Smad1, Smad5, and Smad7 showed opposite trends versus the protein levels upon TXNIP suppression (Figure S12A), suggesting that the effect of TXNIP on these molecules might be a consequence of posttranslational regulation. By contrast, mRNA expression of Smad4 increased markedly upon TXNIP suppression, along with protein levels (Figure S12A). Blockading the proteasome degradation pathway by MG132 effectively abrogated the effect of TXNIP suppression on both Smad1 and Smad5. However, it did not affect Smad7 (Figure S12B), implying that the effect of TXNIP on Smad7 could involve other routes (eg, the lysosomal degradation pathway). We additionally checked the expression of BMP receptor BMPR1A and E3 ubiquitin ligase Smurf1/Smurf2 which can degrade BMP receptors or R-Smads.[37,53] We found that TXNIP suppression did not alter BMPR1A, Smurf1, or Smurf2 levels (Figure S12C). Considering TXNIP is a α-arrestin protein that act as a scaffolding protein in various signaling pathways,[17] TXNIP may directly interact with Smads, Smurf1/2, which are NEDD4 E3s ubiquitin ligase family, or p38, which is reported to directly interact with TXNIP in hematopoietic stem cells.[54] To define the interacting BMP signaling molecules with TXNIP, we transfected primary cultured VSMCs with pCMV3 plasmid to overexpress the HA-tagged TXNIP clone and performed co-immunoprecipitation, and found that Smad1 was clearly co-immunoprecipitated with TXNIP (Figure S12D). However, the interactions between TXNIP and other molecules including Smad5, Smad7, Smad4, Smurf 1/2, and p38 were not clear. Thus extensive further studies using various experimental techniques (eg, double overexpression of TXNIP and predicted target molecules, blue native PAGE, or proximity ligation assay) are required to elucidate the exact role of TXNIP in the integrity of BMP signaling molecules.

For an extended discussions regarding (1) the significance and limitations of in vivo mouse models used in our study, (2) characterization of the osteogenic and chondrogenic populations in mice atheroma, (3) possible roles of TXNIP in other cell types and cardiovascular diseases, see Supplemental Discussion.

In conclusion, we demonstrated that TXNIP is a novel regulator of atherosclerotic calcification by suppressing BMP signaling to inhibit the transition of the modulated VSMCs toward an osteochondrogenic population. We propose that by exploiting the inhibitory role of TXNIP in the osteochondrogenic transition of VSMCs, TXNIP could be a potential therapeutic target for atherosclerotic calcification. We also acknowledge that there are some limitations to the human relevance of the osteochondrogenic population of mice, as cartilage metaplasia is rarely observed in human atheroma.

ARTICLE INFORMATION

Received June 15, 2022; revision received November 9, 2022; accepted November 21, 2022.

Affiliations

Department of Veterinary Pathology, College of Veterinary Medicine, Seoul National University, Korea (S.-H.W., D.-M.G., J.-S.O., D.-Y.K.). Laboratory of Developmental Biology and Genomics, Research Institute for Veterinary Science, College of Veterinary Medicine, Seoul National University, Korea (D.K.). Department of Life Science, College of Natural Sciences, Research Institute of Natural Sciences, Research Institute for Convergence of Basic Sciences, Hanyang Institute of Bioscience and Biotechnology, Hanyang University, Seoul, Korea (S.H.L., K.S.P., M.K., K.K., J.-H.C.). Department of Veterinary Pathology, College of Veterinary Medicine, Chungnam National University, Daejeon, Korea (H.-J.K.). Laboratory Animal Resource Center, Korea Research Institute of Bioscience and Biotechnology (KRIBB), Cheongju, Korea (Y.-S.W., W.K.Y.). Immunotherapy Convergence Research Center, Korea Research Institute of Bioscience and Biotechnology (KRIBB), Daejeon, Korea (I.C.). Enviornmental Diseases Research Center, Korea Research Institute of Bioscience and Biotechnology (KRIBB), Daejeon, Korea (Y.-J.P.). Department of Pathology, Hanyang University Medical College, Seoul, Korea (S.S.P., J.H.K.). Department of Biological Sciences, Research Institute of Women's Health, College of Natural Sciences, Sookmyung Women's University, Seoul, Korea (Y.-H.K.).

Acknowledgments

We acknowledge Dr Dongryeol Ryu and Dr Jong-Sun Kang (Department of Molecular Cell Biology, Sungkyunkwan University School of Medicine) for their help in analyzing public transcriptome. We also thank expert technician Kyeong Hee Kim (Department of Veterinary Pathology, Seoul National University) for technical assistance.

Sources of Funding

This work was supported by the National Research Foundation of Korea funded by the Korean government (grant number NRF-2016M3A-9D5A01952416, 2016M3A9D5A01952413, 2020R1A6A1A06046728, and 2021R1A2C3004586).

Disclosures

None.

Supplemental Materials

Expanded Methods
Figures S1–S12
Tables S1–S11
Supplemental Discussion
References 55–66

REFERENCES

1. Bentzon JF, Otsuka F, Virmani R, Falk E. Mechanisms of plaque formation and rupture. *Circ Res*. 2014;114:1852–1866. doi: 10.1161/CIRCRESAHA.114.302721
2. Libby P. The changing landscape of atherosclerosis. *Nature*. 2021;592:524–533. doi: 10.1038/s41586-021-03392-8
3. Alexopoulos N, Raggi P. Calcification in atherosclerosis. *Nat Rev Cardiol*. 2009;6:681–688. doi: 10.1038/nrcardio.2009.165
4. Greenland P, Bonow RO, Brundage BH, Budoff MJ, Eisenberg MJ, Grundy SM, Lauer MS, Post WS, Raggi P, Redberg RF, et al. ACCF/AHA 2007 clinical expert consensus document on coronary artery calcium scoring by computed tomography in global cardiovascular risk assessment and in evaluation of patients with chest pain: a report of the American College of Cardiology Foundation Clinical Expert Consensus Task Force (ACCF/AHA writing committee to update the 2000 Expert consensus document

on electron beam computed tomography) developed in collaboration with the society of atherosclerosis imaging and prevention and the society of cardiovascular computed tomography. *J Am Coll Cardiol*. 2007;49:378–402. doi: 10.1016/j.jacc.2006.10.001
5. Virmani R, Kolodgie FD, Burke AP, Farb A, Schwartz SM. Lessons from sudden coronary death: a comprehensive morphological classification scheme for atherosclerotic lesions. *Arterioscler Thromb Vasc Biol*. 2000;20:1262–1275. doi: 10.1161/01.atv.20.5.1262
6. Sugane H, Kataoka Y, Otsuka F, Nakaoku Y, Nishimura K, Nakano H, Murai K, Honda S, Hosoda H, Matama H, et al. Cardiac outcomes in patients with acute coronary syndrome attributable to calcified nodule. *Atherosclerosis*. 2021;318:70–75. doi: 10.1016/j.atherosclerosis.2020.11.005
7. Johnson RC, Leopold JA, Loscalzo J. Vascular calcification: pathobiological mechanisms and clinical implications. *Circ Res*. 2006;99:1044–1059. doi: 10.1161/01.RES.0000249379.55535.21
8. Durham AL, Speer MY, Scatena M, Giachelli CM, Shanahan CM. Role of smooth muscle cells in vascular calcification: implications in atherosclerosis and arterial stiffness. *Cardiovasc Res*. 2018;114:590–600. doi: 10.1093/cvr/cvy010
9. Grootaert MO, Bennett MR. Vascular smooth muscle cells in atherosclerosis: time for a re-assessment. *Cardiovasc Res*. 2021;117:2326–2339. doi: 10.1093/cvr/cvab046
10. Ntokou A, Kabir I, Saddouk FZ, Greif DM. *Vascular Embryology and Angiogenesis. Vascular Medicine: A Companion to Braunwald's Heart Disease E-Book*. Elsevier Health Sciences; 2019:1–16.
11. Sinha S, Santoro MM. New models to study vascular mural cell embryonic origin: implications in vascular diseases. *Cardiovasc Res*. 2018;114:481–491. doi: 10.1093/cvr/cvy005
12. Naik V, Leaf EM, Hu JH, Yang HY, Nguyen NB, Giachelli CM, Speer MY. Sources of cells that contribute to atherosclerotic intimal calcification: an in vivo genetic fate mapping study. *Cardiovasc Res*. 2012;94:545–554. doi: 10.1093/cvr/cvs126
13. Jacobsen K, Lund MB, Shim J, Gunnersen S, Füchtbauer EM, Kjolby M, Carramolino L, Bentzon JF. Diverse cellular architecture of atherosclerotic plaque derives from clonal expansion of a few medial SMCs. *JCI Insight*. 2017;2:e95890. doi: 10.1172/jci.insight.95890
14. Pan H, Xue C, Auerbach B, Fan J, Bashore AC, Cui J, Yang DY, Trignano SB, Liu W, Shi J, et al. Single-cell genomics reveals a novel cell state during smooth muscle cell phenotypic switching and potential therapeutic targets for atherosclerosis in mouse and human. *Circulation*. 2020;142:2060–2075. doi: 10.1161/CIRCULATIONAHA.120.048378
15. Kim JB, Zhao Q, Nguyen T, Pjanic M, Cheng P, Wirka R, Travisano S, Nagao M, Kundu R, Quertermous T. Environment-sensing aryl hydrocarbon receptor inhibits the chondrogenic fate of modulated smooth muscle cells in atherosclerotic lesions. *Circulation*. 2020;142:575–590. doi: 10.1161/circulationaha.120.045981
16. Alencar GF, Owsiany KM, Karnewar S, Sukhavasi K, Mocci G, Nguyen AT, Williams CM, Shamsuzzaman S, Mokry M, Henderson CA, et al. Stem cell pluripotency genes Klf4 and Oct4 regulate complex SMC phenotypic changes critical in late-stage atherosclerotic lesion pathogenesis. *Circulation*. 2020;142:2045–2059. doi: 10.1161/CIRCULATIONAHA.120.046672
17. Yoshihara E, Masaki S, Matsuo Y, Chen Z, Tian H, Yodoi J. Thioredoxin/Txnip: redoxisome, as a redox switch for the pathogenesis of diseases. *Front Immunol*. 2014;4:514. doi: 10.3389/fimmu.2013.00514
18. Kim SY, Suh HW, Chung JW, Yoon SR, Choi I. Diverse functions of VDUP1 in cell proliferation, differentiation, and diseases. *Cell Mol Immunol*. 2007;4:345–351.
19. Qayyum N, Haseeb M, Kim MS, Choi S. Role of thioredoxin-interacting protein in diseases and its therapeutic outlook. *Int J Mol Sci*. 2021;22:2754. doi: 10.3390/ijms22052754
20. Byon CH, Han T, Wu J, Hui ST. Txnip ablation reduces vascular smooth muscle cell inflammation and ameliorates atherosclerosis in apolipoprotein E knockout mice. *Atherosclerosis*. 2015;241:313–321. doi: 10.1016/j.atherosclerosis.2015.05.020
21. Ferreira NE, Omae S, Pereira A, Rodrigues MV, Miyakawa AA, Campos LCG, Santos PCJL, Dallan LA, Martinez TL, Santos RD, et al. Thioredoxin interacting protein genetic variation is associated with diabetes and hypertension in the Brazilian general population. *Atherosclerosis*. 2012;221:131–136. doi: 10.1016/j.atherosclerosis.2011.12.009
22. Alvim RO, Santos PCJL, Ferreira NE, Mill JG, Krieger JE, Pereira AC. Thioredoxin interacting protein (TXNIP) rs7212 polymorphism is associated with arterial stiffness in the Brazilian general population. *J Hum Hypertens*. 2012;26:340–342. doi: 10.1038/jhh.2011.102
23. Alsaigh T, Evans D, Frankel D, Torkamani A. Decoding the transcriptome of atherosclerotic plaque at single-cell resolution. *bioRxiv*. Preprint posted online March 4, 2020. doi: 10.1101/2020.03.03.968123
24. Goettsch C, Hutcheson JD, Hagita S, Rogers MA, Creager MD, Pham T, Choi J, Mlynarchik AK, Pieper B, Kjolby M, et al. A single injection of gain-of-function mutant PCSK9 adeno-associated virus vector induces cardiovascular calcification in mice with no genetic modification. *Atherosclerosis*. 2016;251:109–118. doi: 10.1016/j.atherosclerosis.2016.06.011
25. Park HS, Song JW, Park JH, Lim BK, Moon OS, Son HY, Lee JH, Gao B, Won YS, Kwon HJ. TXNIP/VDUP1 attenuates steatohepatitis via autophagy and fatty acid oxidation. *Autophagy*. 2021;17:2549–2564. doi: 10.1080/15548627.2020.1834711
26. Chutkow WA, Patwari P, Yoshioka J, Lee RT. Thioredoxin-interacting protein (Txnip) is a critical regulator of hepatic glucose production. *J Biol Chem*. 2008;283:2397–2406. doi: 10.1074/jbc.M708169200
27. Shankman LS, Gomez D, Cherepanova OA, Salmon M, Alencar GF, Haskins RM, Swiatlowska P, Newman AAC, Greene ES, Straub AC, et al. KLF4-dependent phenotypic modulation of smooth muscle cells has a key role in atherosclerotic plaque pathogenesis. *Nat Med*. 2015;21:628–637. doi: 10.1038/nm.3866
28. Dobnikar L, Taylor AL, Chappell J, Oldach P, Harman JL, Oerton E, Dzierzak E, Bennett MR, Spivakov M, Jørgensen HF. Disease-relevant transcriptional signatures identified in individual smooth muscle cells from healthy mouse vessels. *Nat Commun*. 2018;9:4567. doi: 10.1038/s41467-018-06891-x
29. Wirka RC, Wagh D, Paik DT, Pjanic M, Nguyen T, Miller CL, Kundu R, Nagao M, Coller J, Koyano TK, et al. Atheroprotective roles of smooth muscle cell phenotypic modulation and the TCF21 disease gene as revealed by single-cell analysis. *Nat Med*. 2019;25:1280–1289. doi: 10.1038/s41591-019-0512-5
30. New SEP, Goettsch C, Aikawa M, Marchini JF, Shibasaki M, Yabusaki K, Libby P, Shanahan CM, Croce K, Aikawa E. Macrophage-derived matrix vesicles: an alternative novel mechanism for microcalcification in atherosclerotic plaques. *Circ Res*. 2013;113:72–77. doi: 10.1161/CIRCRESAHA.113.301036
31. Long F, Ornitz DM. Development of the endochondral skeleton. *Cold Spring Harb Perspect Biol*. 2013;5:a008334. Doi: 10.1101/cshperspect.a008334
32. Wolock SL, Krishnan I, Tenen DE, Matkins V, Camacho V, Patel S, Agarwal P, Bhatia R, Tenen DG, Klein AM, et al. Mapping distinct bone marrow niche populations and their differentiation paths. *Cell Rep*. 2019;28:302–311.e5. doi: 10.1016/j.celrep.2019.06.031
33. Haseeb A, Kc R, Angelozzi M, de Charleroy C, Rux D, Tower RJ, Yao L, da Silva RP, Pacifici M, Qin L, et al. SOX9 keeps growth plates and articular cartilage healthy by inhibiting chondrocyte dedifferentiation/osteoblastic redifferentiation. *Proc Natl Acad Sci USA*. 2021;118:e2019152118. doi: 10.1073/pnas.2019152118
34. Rattazzi M, Bennett BJ, Bea F, Kirk EA, Ricks JL, Speer M, Schwartz SM, Giachelli CM, Resenfeld ME. Calcification of advanced atherosclerotic lesions in the innominate arteries of ApoE-deficient mice: potential role of chondrocyte-like cells. *Arterioscler Thromb Vasc Biol*. 2005;25:1420–1425. doi: 10.1161/01.ATV.0000166600.58468.1b
35. Slenders L, Landsmeer LPL, Cui K, Depuydt MAC, Verwer M, Mekke J, Timmerman N, van den Dungen NAM, Kuiper J, de Winther MPJ, et al. Intersecting single-cell transcriptomics and genome-wide association studies identifies crucial cell populations and candidate genes for atherosclerosis. *Eur Heart J*. 2021;2:oeab043. doi: 10.1093/ehjopen/oeab043
36. Chakraborty R, Saddouk FZ, Carrao AC, Krause DS, Greif DM, Martin KA. Promoters to study vascular smooth muscle: mistaken identity?. *Arterioscler Thromb Vasc Biol*. 2019;39:603–612. doi: 10.1161/ATVBAHA.119.312449
37. Wu M, Chen G, Li YP. TGF-β and BMP signaling in osteoblast, skeletal development, and bone formation, homeostasis and disease. *Bone Res*. 2016;4:16009. doi: 10.1038/boneres.2016.9
38. Miyazono K. Id:A target of BMP signaling. *Science's STKE*. 2002;151:pe40. doi: 10.1126/stke.2002.151.pe40
39. Rodríguez-Carballo E, Gámez B, Ventura F. P38 MAPK signaling in osteoblast differentiation. *Front Cell Dev Biol*. 2016;4:40. doi: 10.3389/fcell.2016.00040
40. Garcia-Alonso L, Holland CH, Ibrahim MM, Turei D, Saez-Rodriguez J. Benchmark and integration of resources for the estimation of human transcription factor activities. *Genome Res*. 2019;29:1363–1375. doi: 10.1101/gr.240663.118
41. Sanvitale CE, Kerr G, Chaikuad A, Ramel MC, Mohedas AH, Reichert S, Wang Y, Triffitt JT, Cuny GD, Yu PB, et al. A new class of small molecule inhibitor of BMP signaling. *PLoS One*. 2013;8:e62721. doi: 10.1371/journal.pone.0062721

42. Cai T, Sun D, Duan Y, Wen P, Dai C, Yang J, He W. WNT/β-catenin signaling promotes VSMCs to osteogenic transdifferentiation and calcification through directly modulating Runx2 gene expression. *Exp Cell Res*. 2016;345:206–217. doi: 10.1016/j.yexcr.2016.06.007
43. Wang XQ, Nigro P, World C, Fujiwara K, Yan C, Berk BC. Thioredoxin interacting protein promotes endothelial cell inflammation in response to disturbed flow by increasing leukocyte adhesion and repressing Kruppel-like factor 2. *Circ Res*. 2012;110:560–568. doi: 10.1161/CIRCRESAHA.111.256362
44. Domingues A, Boisson-Vidal C, Rouge PM, Dizier B, Sadoine J, Mignon V, Verssières E, Henrion D, Escriou V, Bigey P, et al. Targeting endothelial thioredoxin-interacting protein (TXNIP) protects from metabolic disorder-related impairment of vascular function and post-ischemic revascularisation. *Angiogenesis*. 2020;23:249–264. doi: 10.1007/s10456-019-09704-x
45. Spindel ON, Burke RM, Yan C, Berk BC. Thioredoxin-interacting protein is a biomechanical regulator of Src activity: key role in endothelial cell stress fiber formation. *Circ Res*. 2014;114:1125–1132. doi: 10.1161/CIRCRESAHA.114.301315
46. Greenblatt MB, Ono N, Arturk UM, Debnath S, Lalani S. The unmixing problem: a guide to applying single-cell RNA sequencing to bone. *J Bone Miner Res*. 2019;34:1207–1219. doi: 10.1002/jbmr.3802
47. Canet-Soulas E, Bessueille L, Mechtouff L, Magne D. The elusive origin of atherosclerotic plaque calcification. *Front Cell Dev Biol*. 2021;9:622736. doi: 10.3389/fcell.2021.622736
48. Qiao JH, Mertens RB, Fishbein MC, Geller SA. Cartilaginous metaplasia in calcified diabetic peripheral vascular disease: morphologic evidence of endochondral ossification. *Human Pathol*. 2003;34:402–407. doi: 10.1053/hupa.2003.72
49. Lin ME, Chen TM, Wallingford MC, Nguyen NB, Yamada S, Sawangmake C, Zhang J, Speer MY, Giachelli CM. Runx2 deletion in smooth muscle cells inhibits vascular osteochondrogenesis and calcification but not atherosclerotic lesion formation. *Cardiovasc Res*. 2016;112:606–616. doi: 10.1093/cvr/cvw205
50. Sun Y, Byon CH, Yuan K, Chen J, Mao X, Heath JM, Javed A, Zhang K, Anderson PG, Chen Y. Smooth muscle cell–specific Runx2 deficiency inhibits vascular calcification. *Circ Res*. 2012;111:543–552. doi: 10.1161/CIRCRESAHA.112.267237
51. Wang Y, Ma WQ, Zhu Y, Han XQ, Liu N. Exosomes derived from mesenchymal stromal cells pretreated with advanced glycation end product-bovine serum albumin inhibit calcification of vascular smooth muscle cells. *Front Endocrinol*. 2018;9:524. doi: 10.3389/fendo.2018.00524
52. Tian L, Wang Y, Zhang R. Galectin-3 induces vascular smooth muscle cells calcification via AMPK/TXNIP pathway. *Aging (Albany NY)*. 2022;14:5086–5096. doi: 10.18632/aging.204130
53. Miyazawa K, Miyazono K. Regulation of TGF-β family signaling by inhibitory Smads. *Cold Spring Harb. Perspect. Biol*. 2017;9:a022095. doi: 10.1101/cshperspect.a022095
54. Jung H, Kim DO, Byun JE, Kim WS, Kim MJ, Song HY, Kim YK, Kang DK, Park YJ, Kim TD, et al. Thioredoxin-interacting protein regulates haematopoietic stem cell ageing and rejuvenation by inhibiting p38 kinase activity. *Nat Commun*. 2016;7:13674. doi: 10.1038/ncomms13674
55. Lee KN, Kang HS, Jeon JH, Kim EM, Yoon SR, Song H, Lyu CY, Piao ZH, Kim SU, Han YH, et al. VDUP1 is required for the development of natural killer cells. *Immunity*. 2005;22:195–208. doi: 10.1016/j.immuni.2004.12.012
56. Vozenilek AE, Blackburn CMR, Schilke RM, Chandran S, Castore R, Klein RL, Woolard MD. AAV8-mediated overexpression of mPCSK9 in liver differs between male and female mice. *Atherosclerosis*. 2018;278:66–72. doi: 10.1016/j.atherosclerosis.2018.09.005
57. Kwon DH, Choe N, Shin S, Ryu J, Kim N, Eom GH, Nam KI, Kim HS, Ahn Y, Kim YK, et al. Regulation of MDM2 E3 ligase-dependent vascular calcification by MSX1/2. *Exp Mol Med*. 2021;53:1781–1791. doi: 10.1038/s12276-021-00708-6
58. Butler A, Hoffman P, Smibert P, Papalexi E, Satija R. Integrating single-cell transcriptomic data across different conditions, technologies, and species. *Nat Biotechnol*. 2018;36:411–420. doi: 10.1038/nbt.4096
59. Boström KI, Yao J, Guihard PJ, Blazquez-Medela AM, Yao Y. Endothelial-mesenchymal transition in atherosclerotic lesion calcification. *Atherosclerosis*. 2016;253:124–127. doi: 10.1016/j.atherosclerosis.2016.08.046
60. Kramann R, Goettsch C, Wongboonsin J, Iwata H, Schneider RK, Kuppe C, Kaesler N, Chang-Panesso M, Machado FG, Gratwohl S, et al. Adventitial MSC-like cells are progenitors of vascular smooth muscle cells and drive vascular calcification in chronic kidney disease. *Cell Stem Cell*. 2016;19:628–642. doi: 10.1016/j.stem.2016.08.001
61. Evrard SM, Lecce L, Michelis KC, Nomura-Kitabayashi A, Pandey G, Purushothaman KR, d`Escamard V, Li JR, Hadri L, Fujitani K, et al. Endothelial to mesenchymal transition is common in atherosclerotic lesions and is associated with plaque instability. *Nat Commun*. 2016;7:1–16. doi: 10.1038/ncomms11853
62. Chen PY, Qin L, Baeyens N, Li G, Afolabi T, Budatha M, Tellides G, Schwartz MA, Simons M. Endothelial-to-mesenchymal transition drives atherosclerosis progression. *J Clin Invest*. 2015;125:4514–4528. doi: 10.1172/JCI82719
63. Tang J, Wang H, Huang X, Li F, Zhu H, Li Y, He L, Zhang H, Pu W, Liu K, et al. Arterial Sca1+ vascular stem cells generate de novo smooth muscle for artery repair and regeneration. *Cell Stem Cell*. 2020;26:81–96.e4. doi: 10.1016/j.stem.2019.11.010
64. Nurnberg ST, Cheng K, Raiesdana A, Kundu R, Miller CL, Kim JB, Arora K, Carcamo-Oribe I, Xiong Y, Tellakula N, et al. Coronary artery disease associated transcription factor TCF21 regulates smooth muscle precursor cells that contribute to the fibrous cap. *PLoS Genet*. 2015;11:e1005155. doi: 10.1371/journal.pgen.1005155
65. Wang RN, Green J, Wang Z, Deng Y, Qiao M, Peabody M, Zhang Q, Ye J, Yan Z, Denduluri S, et al. Bone morphogenetic protein (BMP) signaling in development and human diseases. *Genes Dis*. 2014;1:87–105. doi: 10.1016/j.gendis.2014.07.005
66. Frismantiene A, Philippova M, Erne P, Resink TJ. Smooth muscle cell-driven vascular diseases and molecular mechanisms of VSMC plasticity. *Cell Signal*. 2018;52:48–64. doi: 10.1016/j.cellsig.2018.08.019